Electrochemically Enhanced Antimicrobial Action of Plasma Activated Poly(vinyl alcohol) Hydrogel Dressings

Sumyea Sabrin, Sung-Ha Hong , Sushil Kumar KC , Jun-Seok Oh, Ainslie L.K. Derrick-Roberts , Debabrata K. Karmokar , Habibullah Habibullah , Robert D. Short, Bhagirath Ghimire, Robert Fitridge , Endre J. Szili**

Sumyea Sabrin, Sung-Ha Hong , Sushil Kumar KC, Ainslie L.K. Derrick-Roberts, Endre J. Szili
Future Industries Institute, University of South Australia, Mawson Lakes Campus, Mawson Lakes, South Australia 5095, Australia.
E-mail: ((Sumyea.Sabrin@mymail.unisa.edu.au and Endre.Szili@unisa.edu.au))

Debabrata K. Karmokar, Habibullah Habibullah
UniSA STEM, University of South Australia, Mawson Lakes Campus, Mawson Lakes, South Australia 5095, Australia

Jun-Seok Oh
Graduate School of Engineering, Osaka City University, Osaka 558-8585, Japan

Robert D. Short
Department of Chemistry, The University of Sheffield, Dainton Building, Brook Hill, Sheffield, S3 7HF, UK.

Bhagirath Ghimire
Center for Space Plasma and Aeronomic Research, University of Alabama in Huntsville, Huntsville 35899, USA.
Department of Mechanical and Aerospace Engineering, University of Alabama in Huntsville, Huntsville 35899, USA.

Robert Fitridge
Faculty of Health and Medical Sciences, University of Adelaide, Adelaide, Australia.
Vascular and Endovascular Service, Royal Adelaide Hospital, Adelaide, Australia.

Keywords: electrochemical, reactive species, plasma medicine, plasma jet, chronic wounds, wound healing, poly(vinyl alcohol), hydrogel, wound dressing, plasma activated hydrogel therapy.

This paper presents and explains the principle behind an electrochemical method to enhance the antimicrobial action of plasma activated hydrogel therapy (PAHT) in the context of wound decontamination. The PAHT presented in this paper involves treating poly(vinyl alcohol) (PVA) hydrogel films with a helium (He) plasma jet. During treatment, the PVA hydrogels are grounded and hydrated. This electrochemically enhances the production of hydrogen peroxide (H_2O_2), which is a major antibacterial agent present in the gel. Production of H_2O_2 is shown to be electrically enhanced through electron dissociation reactions, and through reactions associated with excited state species, metastables and UV photolysis. H_2O_2 production is further enhanced through additional hydration of the PVA by spotting water on top of the gel during treatment. Evaporation of the water molecules through the He flow dehydrating the PVA hydrogel fuel the electrochemical dependent reactions associated with H_2O_2 production. The major electrochemical processes that are enhanced are explained through examination of the electrical and optical properties of the He plasma jet during treatment. Overall, the new PAHT approach produces up to an unprecedented 3.4 mM of H_2O_2 in the PVA hydrogel. Production of other molecules such as reactive nitrogen species (RNS) are also enhanced by the same approach. The electrochemically enhanced plasma activated PVA hydrogels are shown to be highly effective at eradicating common wound pathogens *Escherichia coli* and *Pseudomonas aeruginosa* and mildly effective against *Staphylococcus aureus*. Therefore, the approach of using plasma activated PVA hydrogels presented in this study provides a new dressing option for controlling infection in wounds and an alternative to antibiotics and silver-based therapies.

1. Introduction

Chronic wound infections are a silent pandemic threatening to become a global healthcare crisis. The cost of managing chronic wounds such as diabetic foot ulcers (DFUs) is estimated at US$17 billion per year, which is higher than USA's five most costly cancers [1]. The challenge is global with current prediction that by 2030 there will be 578 million people with diabetes (36% increase from 2020), and more than 30% of those with diabetes will experience an ulcer during their lifetime and 60% of these ulcers will become infected. This escalating

problem is caused by antimicrobial resistance (AMR) and by 2050, AMR is forecasted to cause 10 million deaths annually resulting in a potential US$100 trillion shock to the global economy [2]. Increased antibiotic use might see AMR spiral out of control by fuelling antibiotic pollution, devastating the natural environment, and creating major environmental reserves of AMR[3,4].

Unfortunately, management of chronic wounds is predominantly reliant on a limited number of options. These include low-tech manual debridement and low-cost dressing protection, or alternatively high-tech and high-cost antimicrobial dressings and medicinal products [5–11]. All tackle only a single element of the problem. Severe infections require systemic antibiotics and amputation when all else fails.

Low-temperature atmospheric-pressure plasma is emerging as an exciting new technology to control infection and stimulate healing of recalcitrant wounds. The benefit of plasma has been demonstrated in clinical trials showing that plasma treatment reduces bacterial load in wounds [12] and stimulates healing[13] without long-term adverse side-effects[14]. Therefore, plasma is unlike any other wound treatment because of its dual action in controlling infection and stimulating healing. This is most often attributed to the unique and complex mixture of reactive oxygen species (ROS) and reactive nitrogen species (RNS), collectively known as reactive oxygen and nitrogen species (RONS), generated by plasma [15].

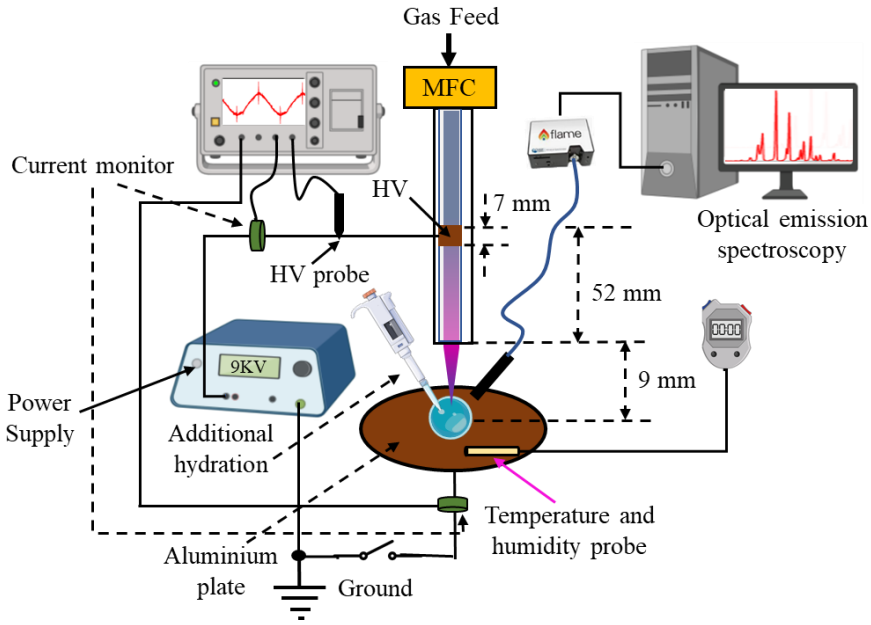

Figure 1. Experimental set-up used to activate the PVA hydrogels with a helium plasma jet. Part of this image was created with biorender.com, and bioiconics.com.

RONS are formed when the plasma effluent mixes with the oxygen, nitrogen and water vapour molecules in the ambient air. The high energy plasma components in the plasma effluent, particularly high energy electrons, ions, electric field and ultra-violet (UV) photons, activate the air molecules forming RONS. RONS generated by plasma in biological environments can intervene in a myriad of signalling processes important in controlling growth of bacteria and human cells [12,13,16]. Particularly, hydrogen peroxide (H_2O_2) and nitrogen oxides (NO_x) are beneficial because of their relatively long lifetime (days) in biological environments, and because these molecules have both bactericidal and growth promoting properties important for decontaminating and healing wounds [17–21].

Complimentary to existing plasma treatments, a new form of plasma therapy is concurrently being developed referred to as plasma activated hydrogel therapy (PAHT) [22]. PAHT involves loading plasma generated RONS into a hydrogel either by treating a hydrogel directly with plasma or forming a hydrogel with plasma treated solution. This enables the longer-lived plasma generated molecules such as H_2O_2 and NO_x to be stored within the hydrogel before application to a biological target. The use of liquid H_2O_2 in the clinic is commonplace. However, the use of liquids, particularly with complex chronic wounds, can be quite tricky, and dose is not easily controlled (which can be with PAHT). Moreover, it has been shown that the unique chemical composition produced by plasma is significantly more effective at killing microorganisms than any of its single molecular components (e.g. H_2O_2) [23,24].

When the hydrogel is placed on top of a target (e.g., a wound) the molecules are subsequently eluted from the hydrogel and onto the target to treat the disease. PAHT is at its early stage of investigation and could prove promising for treatment of different diseases such as fungal infections [24], vitiligo [25],and osteosarcoma [18,22,26,27].
More recently, PAHT has been applied for decontamination of pathogenic bacteria commonly found in wounds [12–14]. PAHT is particularly useful for wound treatment because it can be easily integrated with clinical workflows where various dressings are currently used to protect, decontaminate, and heal wounds. PAHT may become a significant innovation in wound dressing technologies because of problems faced with current state-of-the-art silver dressings including growing concerns over silver-induced toxicity and impaired healing [28,29]. With escalating problems of AMR, new dressing products are urgently needed. PAHT can be considered at the frontier of emerging new wound dressing products because of its potential to decontaminate and promote healing. H_2O_2 is particularly a useful molecule for wound treatment because of its broad-spectrum bactericidal properties for decontamination and

because it can stimulate cell growth for healing. However, a significant limitation of PAHT is that it is difficult to load and retain the plasma generated molecules (such as H_2O_2) in the hydrogel at concentrations high enough to be beneficial for wound treatment. Higher RONS concentrations are potentially needed to successfully decontaminate bacterial biofilms commonly formed on slow healing wounds, which have been shown to resist plasma treatments [30–34]. Biofilm resistance to RONS is attributed to the bacteria releasing an antioxidant defence enzyme catalase that neutralises H_2O_2 within the biofilm [34]. Furthermore, higher H_2O_2 concentrations in the mM range are required to stimulate healing *in vivo* [18]. Previously it has been reported that concentrations of H_2O_2 in the range of 10-350 μM can be generated in PAHT [27,35–37]. Whilst it is difficult to directly compare the concentrations of RONS used in PAHT because of the different sizes of the hydrogels used in these studies, it is likely that higher concentrations of topical applications of RONS in the mM range will be needed to achieve decontamination in patients having complex wounds and biofilm infections that enhance resistance of bacteria to antiseptic treatments [38,39]. Therefore, it is important to develop procedures that can produce hydrogel dressings with realistic doses of RONS and other plasma generated molecules relevant for clinical (i.e., real patient) treatment of wounds.

This paper describes a process of activating PAHT dressings with unprecedented high concentrations of H_2O_2 in the mM range. Poly(vinyl alcohol) (PVA) is chosen for this study because of its widespread regulatory approval for healthcare uses and its excellent mechanical and biocompatibility properties for use in wound dressing products [40]. In addition, the high ionic conductivity of PVA promotes electrochemical reactions initiated by plasma treatment [41]. Incorporating H_2O_2 into PVA would be challenging because PVA cannot be melted below ~ 200^0C that is likely to degrade H_2O_2 because it is heat sensitive. This can be overcome by activating PVA with plasma, which has additional advantages of being a dry process (suited to the clinic) and that H_2O_2 is generated "on demand" by the plasma and the amount generated is controlled by the plasma treatment time.The process involves incorporating the hydrogel into the electrical circuit of a plasma jet in a humidified atmosphere that enhances H_2O_2 production through electron dissociation reactions and UV photolysis. The paper focuses on the physics and chemistry underpinning the new treatment procedure and its benefits in treatment of common bacterial pathogens present in wounds.

2. Materials and methods

2.1. Fabrication of poly(vinyl alcohol) (PVA) hydrogel

The hydrogel was prepared from PVA powder (Catalogue number: 9002-89-5, Sigma-Aldrich Corporation). The PVA powder was mixed with clinical grade irrigation water (IW, Model number: AHF7114 – Baxter) to a concentration of 8% (w/v). This percentage of PVA was determined to be optimal for PAHT (in terms of structural integrity and RONS loading) based on preliminary studies. The mixture was heated to 200^0C for 2h on a hot plate with constant stirring using a magnetic stirring bar until the PVA powder was completely dissolved. Afterwards, 5 mL of the mixture was dispensed into a 60 mm diameter polystyrene petri dish and incubated overnight in the freezer at -18^0C to crosslink the gel. The frozen mixture was then allowed to defrost at ambient room temperature. This procedure produced a PVA hydrogel of ~1 mm thickness. A biopsy punch (Acu-Punch Biopsy Punch, EBOS, Kingsgrove, NSW, Australia) was used to cut 10 mm diameter discs of the PVA hydrogel for experiments.

2.2. Plasma treatment of PVA hydrogel

The plasma jet experimental set-up used to treat the PVA hydrogels is shown in Figure 1. The plasma jet assembly consists of a 110 mm long silica tube with an inner diameter of 2 mm and outer diameter of 6 mm tapered at the orifice to 200 µm. A 7 mm long hollow copper electrode wrapped around the silica tube at distance of 45 mm from the tube's orifice served as the high voltage (HV) electrode.

The PVA hydrogel was positioned above an aluminum (Al) plate 9 mm from the orifice of the silica tube so that the plasma plume remained in contact with it during treatment. The PVA hydrogel was kept at floating potential or grounded by either disconnecting the Al plate from ground or connecting to a grounded wire, respectively. A helium (He) plasma jet was ignited by purging 0.5 standard liters per minute (SLPM) He gas through the silica tube with a digital mass flow controller (Model number: AX-MC-2SLPM-D/5M, Apex) and applying 9 kV_{p-p} at 30 kHz to the HV electrode with a high voltage power supply (Model number: PVM500, Information Unlimited), as previously described [42–46]. Different combinations of plasma treatments were performed with the PVA hydrogel at floating potential or grounded with and without additional hydration by pipetting 40 µL of IW on top of the PVA hydrogel at regular 1 min intervals throughout the treatment as listed in Table 1. To understand if RONS production in the PVA hydrogels could be electrochemically enhanced, PVA hydrogels were

activated by the He plasma jet by either placing them above the grounded Al plate or non-grounded Al plate (i.e., at floating potential), with and without additional hydration (Table 1). H_2O_2 and NO_2^- were used as markers to estimate release of ROS and RNS, respectively, from the PVA hydrogels as previously described [47–49].

Table 1. Experimental conditions used to evaluate how production of RONS are electrochemically enhanced in the PVA hydrogel.

PVA	Ground (GND) or floating (FLT) potential	Additional hydration (W)	Acronym
No PVA	FLT	-	No PVA-FLT
No PVA	GND	-	No PVA-GND
PVA	FLT	-	PVA-FLT
PVA	FLT	W	PVA-FLT-W
PVA	GND	-	PVA-GND
PVA	GND	W	PVA-GND-W

2.3. Plasma treatment characterization

2.3.1. Electrical characterization

The electrical properties of the He plasma jet in contact with the target grounded or at floating potential was characterised by measuring the current-voltage signals as represented in Figure 1. Voltage and current waveforms were measured using a HV probe (Model number: HVP39pro, Pintek) and a current monitor (Model number: 2877, Pearson Electronics Inc.), respectively, and were recorded on an oscilloscope (Model number: DSO6034A, Agilent).

Dissipated power (P) during the discharge was calculated through the integration of current and voltage signals over one discharge cycle as: [50],

$$P = f \int_{t=0}^{t=T} I(t)V(t)dt \quad (1)$$

Here, $I(t)$, $V(t)$, T, and f represents total current, voltage, time-period, and frequency of the system, respectively. The current peak in the rising part of the applied voltage was then used to calculate the maximum accumulated charges (Q) as: [50]

$$Q = \int_{t_1}^{t_2} I(t)dt \quad (2)$$

Here, t_1 and t_2 represents the start and end time of the discharge current peak, respectively.

2.3.2. Optical emission characteristics

Optical emission spectra (OES) of the plasma jet were measured using an Ocean Optics HR4000CG-UV-NIR spectrometer equipped with an optical fiber of diameter 600 μm and a collimated lens at the end of the fiber tip to efficiently capture light. The spectra were measured 9 mm below the silica tube with the optical fiber aimed towards the plasma jet – PVA hydrogel interface. The integration time of the spectrometer was set to 100 ms. Absolute irradiance spectroscopy was utilized to measure the photon energy density at 309 nm which also corresponds to the emission from the hydroxyl radical ($^{\bullet}$OH). For these measurements a Deuterium-halogen radiation source (DH-3 plus) was used to calibrate the spectrometer. The absolute irradiance at a specific wavelength (I(λ)) was calculated by subtracting the intensity of the dark spectrum (D(λ)) from the intensity of the sample spectrum (S(λ)). The I(λ) was calculated from Equation 3 [51]:

$$\mathrm{I}(\lambda) = \frac{\mathrm{S}(\lambda) - \mathrm{D}(\lambda)}{\tau \times \mathrm{A} \times \mathrm{d}\lambda} \times \mathrm{C}(\lambda) \quad (3)$$

Here, τ is the integration time of the spectrometer (set to 100 ms), A is the collection area of the cosine corrector (37 mm^2), dλ is the wavelength spread (1 nm), and C(λ) is the calibration data at the specific wavelength provided by the manufacturer. The photon energy density of the plasma jet was calculated by multiplying I (λ) in Equation 3 by the integration time of the spectrometer and was expressed in the unit of mJ/m^2.

2.4. Measurement of environmental parameters

Humidity and temperature in the air 20 mm from the plasma jet – PVA hydrogel interface were measured using humidity (Model number: HT-3006HA, Lutron) and temperature (Model number: HT-3006HA, Lutron) probes, respectively.

2.5. Characterization of plasma treated PVA

2.5.1. Swelling ratio

Swelling ratio of the PVA hydrogel discs was measured following incubation in 1 mL of IW for 1, 2, 3, 4 and 24 h. Swelling ratio was calculated from Equation 4.

$$Swelling\ ratio = \frac{m_t - m_0}{m_0} \times 100\% \quad (4)$$

Where m_0 and m_t is the weight of the PVA hydrogel discs before and after incubation in the IW, respectively.

2.5.2. Release of H_2O_2 and NO_2^-

Plasma treated PVA hydrogels were incubated in 600 µL IW in a 48-well plate for 3 h to study release of H_2O_2 and NO_2^-, which were used as markers for total ROS and RNS, respectively, as previously described [52–56].

H_2O_2 concentration was calculated by measuring the oxidation of o-phenylenediamine (OPD) mixed with horseradish peroxidase (HRP). In the presence of H_2O_2, HRP catalyses the oxidation of OPD to form 2-3-diaminophenazine with an absorbance maximum of 450 nm. The OPD-HRP stock was prepared by dissolving a tablet of OPD (Catalogue number: 9003-99-0, Sigma-Aldrich) into 10 mL of IW. Then, 20 µL of 5 mgL^{-1} HRP (Catalogue number: 95-54-5, Sigma-Aldrich) was added to the dissolved OPD. Following incubation of the PVA hydrogels in the IW, a 100 µL aliquot was mixed with 100 µL of OPD-HRP stock in a 96-well plate and incubated for 30 min in the dark before measuring the absorbance of the solution at 450 nm in a microplate reader (Molecular Devices, SpectraMax M2).

NO_2^- concentration was calculated by measuring the oxidation of Griess reagent. In the presence of NO_2^-, Griess reagent is oxidised into a diazonium salt, which readily couples with N-(1-naphthalenediamine) to form a highly coloured azo dye with an absorbance maximum of 492 nm. A stock of Griess reagent (Catalogue number: 6000-43-7, Sigma-Aldrich) was prepared by dissolving 50 mg of Griess reagent per 1 mL of IW. Following incubation of the PVA hydrogels in the IW, a 100 µL aliquot was mixed with 100 µL of the Griess reagent stock in a 96-well plate and incubated for 30 min in the dark before measuring the absorbance of the solution at 492 nm in the microplate reader.

Concentrations of H_2O_2 and NO_2^- were calculated from calibrations curves (shown in Figure S1 of the supplementary material).

2.5.3. pH measurement

Following incubation of the PVA hydrogels in the IW (as described above), a 15 µL aliquot was pipetted onto pH strips. Both broad range pH 1-14 (SKU number: PH0114-3-1V-100, Precision Labs, Inc.) and narrow range pH 3-6 (SKU number: PH3060, Precision Labs, Inc.) strips were used to cross-validate measurements. After allowing a few seconds for the pH to completely wet, the excess water was shaken off and the pH recorded using the coloured chart supplied by the manufacturer.

2.5.4. Oxidation potential

An agarose film used to mimic a physical hydrated barrier (similar to what would be encountered by a real biological tissue target such as skin) as previously described [52,53], was used to monitor the oxidation potential of the plasma treated PVA hydrogels. To make the agarose film, a 2% (w/v) agarose solution was first prepared by dissolving agarose (Catalogue number: 9012-36-6, Sigma-Aldrich) into IW by heating in a microwave oven. A 1% (w/v) starch solution was then made by dissolving starch (Catalogue number: 9005-25-B, Sigma-Aldrich Corporation) into IW by heating the solution to boiling point on a hot plate. The solution was then allowed to cool to ambient room temperature. Potassium iodide (KI, Catalogue number: 7681-11-0, company) was added to a concentration of 0.6% (w/v) into the cooled starch solution. Then, 20 ml of a 50:50 mixture of the agarose and KI-starch solutions were poured into a 90 mm petri dish. The solution was set by allowing to cool to ambient room temperature. KI is used as an indicator of RONS. RONS oxidize KI generating triiodide ions that form a purple coloured product in the presence of starch that is easily visible by eye [55]. Experiments were performed by placing the PVA hydrogel samples on top of the agarose film for 15 min before removing and visualizing the colour change on the agarose film. A darker purple colour in the agarose tissue film indicates that a higher concentration of RONS was transferred from the PVA hydrogel.

2.6. Antimicrobial assays

Bactericidal efficacy of the plasma treated hydrogels was assessed by zone of inhibition (ZOI) of bacterial lawns [57]. Gram-negative *Escherichia coli* (*E. coli*) [ATCC 11303] and *Pseudomonas aeruginosa* (*P. aeruginosa*) [PA14], and Gram-positive *Staphylococcus aureus*

(S. aureus) [ATCC 25923] were used for this study. *E. coli* and *P. aeruginosa* were grown in 5 mL Luria–Bertani broth (LB) and *S. aureus* in Tryptic Soy Broth (TSB) at 37°C in an orbital shaker overnight. Optical densities of the inoculum were measured at 600 nm to estimate bacteria concentration. Bacteria cultures were serially diluted with LB or TSB media until an optical density (OD) at 600 nm of 0.6 was achieved, which corresponded to a bacteria concentration of 1 x 10^8 cells mL^{-1} based on measurements in our laboratory. LB and TSB agar plates (90 mm diameter) were prepared by dissolving LB and TSB agar powder, respectively, in Milli-Q water. The solutions were autoclaved and allowed to cool. When the temperature cooled to ~ 50°C, 20 mL of the solution was poured into a 90 mm petri dish. After the agar was set, the plates were stored refrigerated at 4^0C before use. The bacteria cultures were diluted to 1 x 10^6 cells mL^{-1} before evenly spreading 100 µL onto the plates and incubating at ambient room temperature for 5 min inside a biosafety cabinet. Plasma treated and untreated (control) PVA hydrogels were placed in the centre of the bacterial lawns. The samples were incubated statically at 37^0C for 24 h. Photographs of the plates were taken for analysis. The area of the ZOI was measured with ImageJ 1.53 image processing software (NIH, USA). ZOI values were normalised according to Equation 5:

$$Normalised\ ZOI = \frac{Area\ of\ the\ bacteria\ ZOI\ (mm^2)}{Area\ of\ the\ sample\ (mm^2)} \quad (5)$$

2.7. Skin cell viability assay

Human immortalised keratinocytes (HaCaTs, ATCC, Virginia, USA) and human foreskin fibroblast (HFFs, CellBank Australia, NSW, Australia) were maintained and cultured in Dulbecco's Modified Eagle Medium (DMEM) (Thermo Fisher Scientific, VIC, Australia) supplemented with 10% (v/v) heat-inactivated fetal bovine serum (FBS) (Thermo Fisher Scientific, VIC, Australia), 1% (v/v) L-glutamine (200 mM) (Thermo Fisher Scientific, VIC, Australia) and 1% (v/v) penicillin/streptomycin (5000U/mL) (Thermo Fisher Scientific, VIC, Australia). HaCaT keratinocyte and HFF cells were passaged by trypsinization, which involved incubation at 37°C with trypsin−Ethylenediaminetetraacetic acid (EDTA) (0.25% w/v in PBS) for 5 min. Trypsin was neutralised by adding equal volumes of cell culture media before transferring to a centrifuge tube and centrifuging at 1500 rpm for 5 min. The cell pellet was resuspended in cell culture media in preparation for counting and seeding into plates for

the cell viability experiments. Cell concentration was measured by mixing 20 µL of trypan blue with a 20 µL aliquot of the cell suspension and pipetting into cell counting slides, which were counted using an automated cell counter (Luna-II, Logos Biosystem, South Korea). HaCaT and HFF cells were seeded at a density of 12.5 x 10^4 cells/cm^2 and 7.8 x 10^4 cells/cm^2 in 96-well plates, respectively. Cells were cultured at 37°C in a 5% CO_2 atmosphere for 24 h prior to performing the cell viability experiments.

Cell viability was performed using resazurin. Metabolic products released from living cells convert non-fluorescent resazurin into a fluorescent product. Plasma treated and untreated PVA hydrogels were incubated in 1 mL of cell culture media for 3 h under cell conditions. This time was sufficient to allow for release of RONS and other plasma generated molecules from the PVA hydrogels. This media was then used to assess the cell viability response. The experiment involved first aspirating the cell culture media from the cells that had been incubated in the 96-well plates, washing with PBS, and then replacing with 100 µL of the cell culture media that had been incubated with the PVA hydrogels. The cells were then incubated for a further 24 h and 48 h before performing the cell viability experiment. To perform the cell viability experiment, the test cell culture media was aspirated from the cells and the cells were washed with PBS. Then, a 100 µL aliquot of 10% (w/v) resazurin (Thermo Fisher) prepared in cell culture media was added to the cells and incubated under cell culture conditions for 1 h. The fluorescence was measured using the microplate reader (same model as provided above) at excitation and emission wavelengths of 555 nm and 585 nm, respectively. The results were derived from the average of two replicates per experiment and two experimental repeats. Percentage of cell viability was calculated by dividing the test cell group by the cells grown in the untreated cell culture media.

2.8. Statistical analysis

Statistical analysis was performed on the relevant data using an unpaired Student t-test assuming unequal variances. A p value of less than 0.05 was considered to be significantly different (at least 95% confidence). Data was processed using GraphPad Prism 10 software.

3. Results and discussion

3.1. Physical characteristics of PAHT

An 8% (w/v) PVA hydrogel was determined to be optimal as a PAHT dressing because it could be readily activated by plasma generated RONS whilst still retaining its structural integrity, conformability and ability to swell. All these characteristics are beneficial for a wound dressing. For example, the PVA hydrogel can be easily conformed to a non-planar

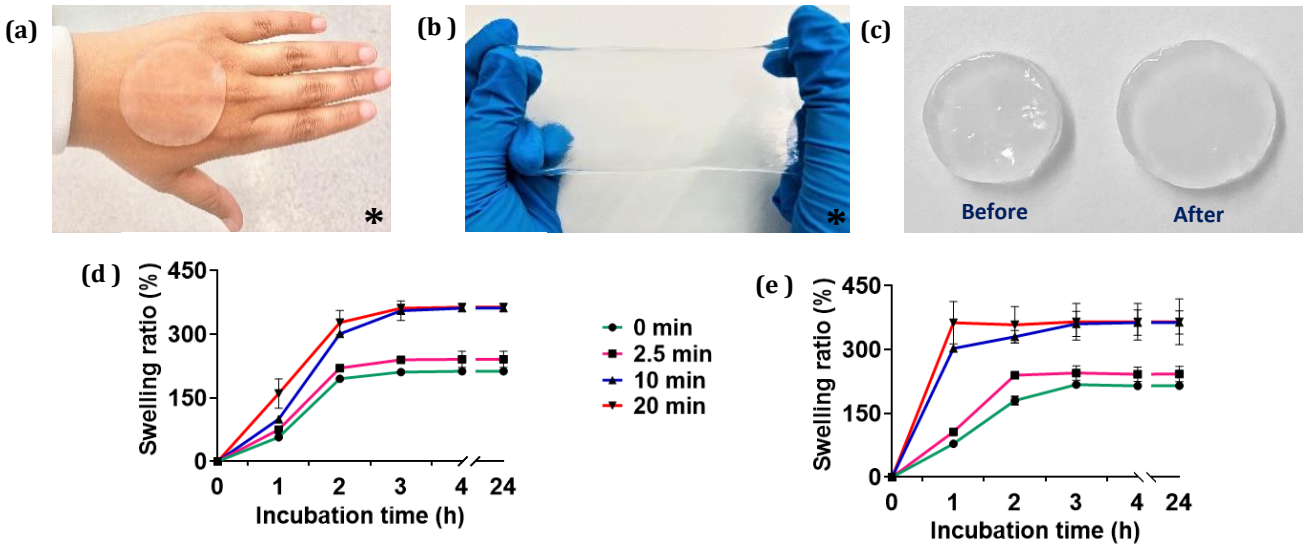

Figure 2. Physical characteristics of the PVA hydrogel including (a) conformability, (b) stretchability, and (c) swelling before and after incubation in water. Quantified swelling ratios are also shown for the untreated PVA hydrogels (0 min) and for the plasma treated PVA hydrogels at (d) floating potential (PVA-FLT) and (e) grounded (PVA-GND) with plasma treatment times of 2.5, 10 and 20 min (n = 3). * Larger sections of PVA hydrogels than used in the experiments are shown in (a) and (b) for clarity.

target (Figure 2 (a)) and be easily stretched without tearing (Figure 2(b)). PVA hydrogels also readily swell as shown in Figure 2 (c), which can be useful for absorbing wound exudate and for promoting transfer of RONS into the wound. Compared to untreated PVA (0 min), plasma treated PVA hydrogels at floating potential (Figure 2(d)) and grounded (Figure 2 (e)) display similar levels of enhanced swelling. This result is attributed to the He gas flow from the plasma jet evaporating water from the entire PVA hydrogel with more evaporation occurring at the centre (of the hydrogel) where the plasma jet contacts its surface. Therefore, more water will evaporate from the PVA hydrogel as the plasma treatment time is increased. In this study, water evaporation from the PVA hydrogel ranged from 18% for 2.5 min of plasma treatment up to 65% for the 20 min treatment. This increases the ability of the hydrogel to swell. Swelling ratio is not affected by grounding the PVA hydrogel (Figure 2 (e) and (d)).

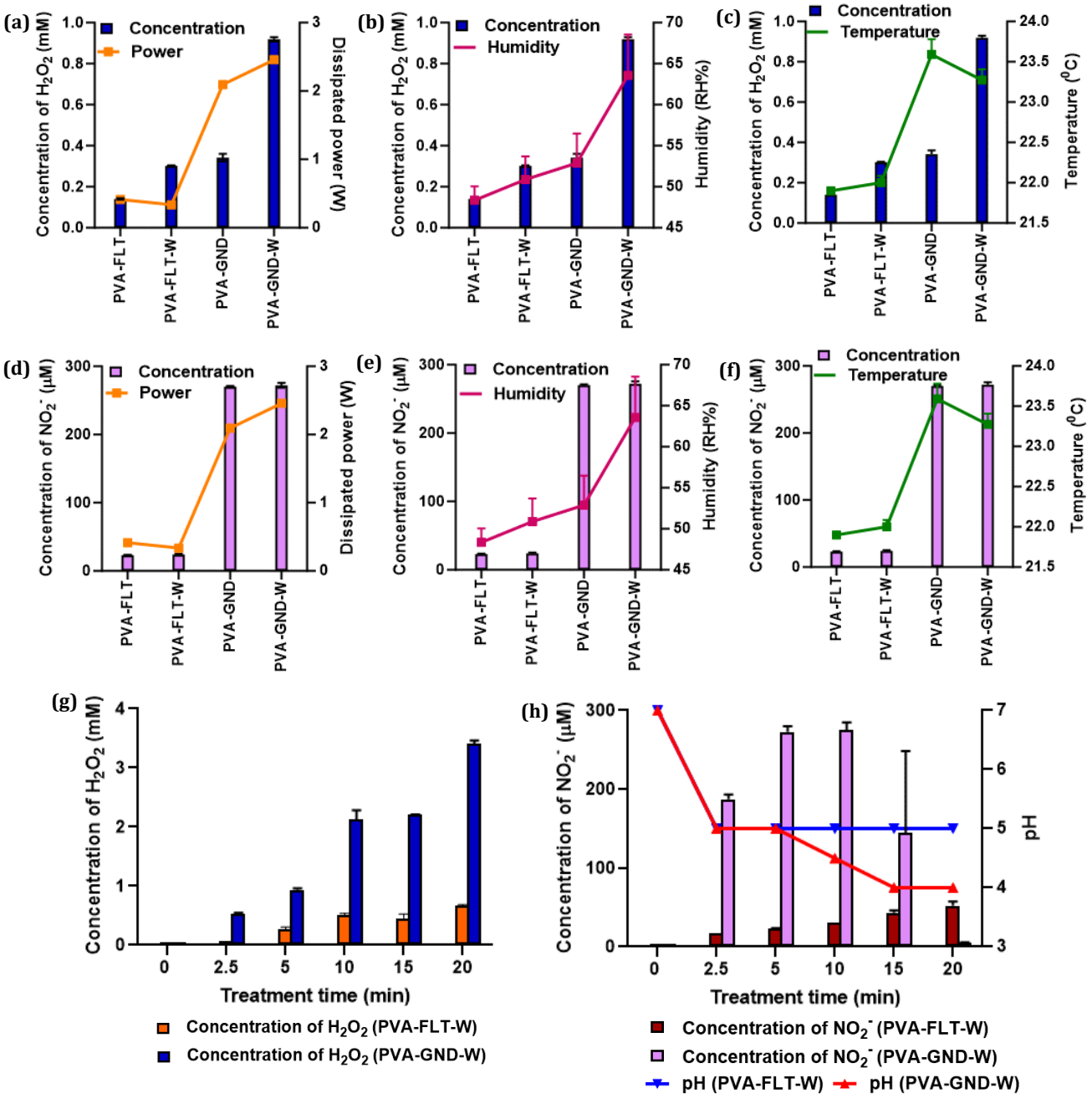

Figure 3. Relationship of H_2O_2 released from the 5 min plasma treated PVA hydrogels with (a) dissipated power, (b) humidity, and (c) temperature, and relationship of NO_2^- released from the plasma treated PVA hydrogels with (d) dissipated power, (e) humidity, and (f) temperature (n = 3). To clearly illustrate the relationship between the different parameters some of the data are duplicated between Figures (a) – (f). (g) H_2O_2, and (h) NO_2^- release from PVA hydrogels following plasma treatment for PVA-FLT-W and PVA-GND-W hydrogels at varying treatment times up to 20 min (n = 3). (h) Also shows the change in pH of the solution used to measure the release of NO_2^-.

3.2. Release of H_2O_2 and NO_2^-

Figure 3 (a), (b) and (c) shows how the plasma dissipated power, humidity and temperature, respectively, influences the concentration of H_2O_2 that can be produced and subsequently released from the plasma treated PVA hydrogels. It is obvious that grounding the PVA during plasma treatment enhances H_2O_2 release, and that release of H_2O_2 is further enhanced by hydrating the PVA hydrogel during treatment. This treatment approach (PVA-GND-W) results in a 5-fold increase in production of H_2O_2 when compared to the PVA hydrogel treated at floating potential (PVA-FLT). Grounding the PVA during plasma treatment also increased the dissipated power of the plasma discharge. The effect of grounding is to promote production of high energy components that enhances H_2O_2 production [58,59,47]. However, H_2O_2 production is not solely controlled by dissipated power because additional hydration of the PVA further enhanced H_2O_2 production without significantly increasing dissipated power (Figure 3(a)). In addition to dissipated power, humidity was also found to be an important parameter because increased humidity at the plasma jet – PVA hydrogel interface closely correlated with increased H_2O_2 production (Figure 3(b)). Temperature at the plasma jet – PVA hydrogel interface was maintained below 24°C and varied by less than 2°C for all treatments (Figure 3(c)). Therefore, temperature was unlikely to have a major impact in production of H_2O_2 (and other RONS) in these experiments.

The concentration of NO_2^- released from the plasma treated PVA hydrogel dressings and its correlation to plasma dissipated power and the humidity and temperature in the surrounding environment is shown in Figure 3 (d), (e) and (f), respectively. Grounding the PVA during plasma treatment significantly enhanced the concentration of NO_2^- that could be subsequently released from the hydrogel. However, hydrating the PVA hydrogel had negligible effect on NO_2^- release. Increased NO_2^- release from the PVA closely correlated with increasing dissipated power but the correlation with humidity was less evident.

The next experiments were performed to analyse the maximum concentrations of H_2O_2 and NO_2^- that could be produced with the PVA hydrogel treated at floating potential and grounded with regular hydration (PVA-FLT-W and PVA-GND-W) as a function of plasma treatment time. Plasma treatment times were varied up to 20 min. Figure 3 (g) shows that a significantly higher concentration of H_2O_2 was released from the PVA hydrogels that were grounded during treatment. Over 3 mM of H_2O_2 was released from the PVA-GND-W hydrogel treated for 20 min with the plasma jet. This is significantly higher compared to only 0.7 mM H_2O_2 released from the PVA-FLT-W hydrogel that was plasma treated for the same time. Figure 3

(h) shows the maximum concentrations of NO_2^- that could be released from the PVA hydrogels prepared using the same conditions. A maximum of 275 μM NO_2^- was released from the PVA-GND-W hydrogel prepared with 10 min of plasma treatment. But PVA-GND-W treated for longer times of 15 and 20 min released significantly lower concentrations of NO_2^-. Conversely, the trend in the concentration of NO_2^- released from the PVA-FLT-W hydrogels increased as function of treatment time. However, these PVA hydrogels released significantly lower concentrations of NO_2^- with a maximum release of only 52 μM for the PVA hydrogels treated for 20 min. The higher concentration of NO_2^- released from PVA hydrogels that were grounded compared to kept at floating potential during plasma treatment can be explained by the differences in the electrical circuits of the plasma treatment system. Grounding provides a direct path for current to flow that increases the dissipated power of the plasma discharge. This promotes production of NO_2^- through electron impact reactions, which will be described later in Equation 15-17. However, NO_2^- can also react with the plasma generated H_2O_2 to form peroxynitrous acid (ONOOH) through Equation 6 [47,48,60].

$$NO_2^- + H_2O_2 + H^+ \rightarrow ONOOH + H_2O \quad (6)$$

To understand if this might have occurred, the pH of the solutions used to measure the release of the NO_2^- was also monitored in Figure 3 (h). For the PVA-FLT-W hydrogels the solution pH plateaus to pH 5 with respect to plasma treatment time. Whereas for the PVA-GND-W hydrogels where higher concentrations of H_2O_2 and NO_2^- were produced, the solution pH continues to decrease to pH 4. Therefore, this result suggests that NO_2^- is being consumed as more ONOOH is produced. This can explain the negative parabolic relationship between NO_2^- release and treatment time for the PVA-GND-W hydrogels.

3.3. Electrochemical enhancement of RONS production

3.3.1. Electrical enhancement through grounding

Figure 4 shows the current (I) and voltage (V) waveforms of the He plasma jet for the experimental conditions described in Table 1. As can be seen in Figure 4 (a) the comparison between grounding and floating conditions, grounding the Al plate significantly enhances the discharge current. This is due to the establishment of a conducting path between the high voltage and the ground electrode. For the No PVA-GND condition, a prominent positive

current peak and small negative current peak is visible. This corresponds to one major positive discharge and one minor negative discharge, which is commonly seen in dielectric barrier discharge (DBD) plasma jets [61–63]. Connecting the PVA hydrogel into the electrical circuit of the plasma treatment system decreases the discharge current even if the PVA is at floating potential (Figure 4 (b)). The reason for this is that the PVA hydrogel is adding resistance between the conducting plasma jet and Al plate in the electrical circuit.

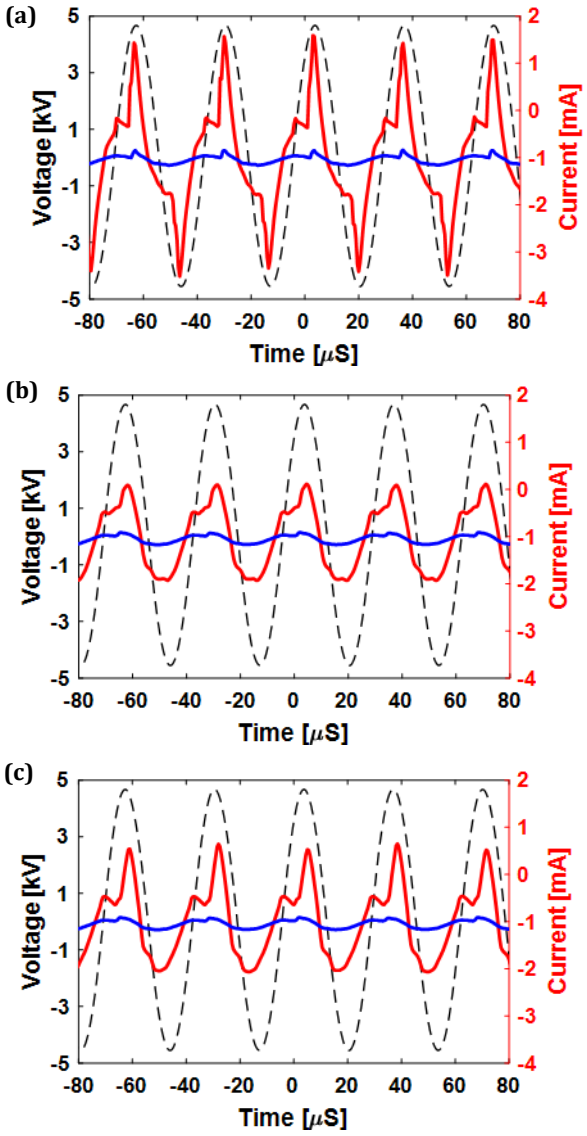

Figure 4. I-V plots measured for the He plasma jet with (a) No PVA, (b) PVA, (c) PVA-W with grounding (solid red curves) and floating (solid blue curves) conditions. Applied voltage is represented by the dashed black curve.

Grounding the PVA further increases the discharge current because it enables a direct pathway of electron flow (Figure 4 (b)). From Table 2 it is clear that grounding the circuit of the plasma treatment system without and with the inclusion of the PVA hydrogel, increases

the maximum accumulated charges compared to the treatment conditions at floating potential. This can be visualized by a more intense plasma jet being produced when the AL plate is grounded (Figure 5 (b)) compared to when it is disconnected from ground (Figure 5 (a)). This result is expected to correlate with a greater density of higher energy state species in the plasma jet important for RONS production. Additional hydration of the PVA hydrogel increases the maximum accumulated charges and consequently the dissipated power when the PVA is grounded. The reason behind this result is that additional hydration increases the humidity due to increased evaporation of water, enabling increased absorption and more even distribution of the charges in the air produced by the plasma jet into the PVA hydrogel.

Table 2. Electrical characteristics of the He plasma jet during treatment of the PVA hydrogel.[a]

Treatment conditions	Maximum Accumulated Charges [nC]	Total dissipated power [W]
No PVA-FLT	0.22±0.01	0.48±0.01
No PVA-GND	9.67±0.19	2.88±0.06
PVA-FLT	0.18±0.01	0.39±0.02
PVA-FLT-W	0.18±0.00	0.34±0.01
PVA-GND	5.25±1.05	2.09±0.14
PVA-GND-W	7.87±0.02	2.46±0.02

[a] ± represents standard error of the mean.

A summary of the maximum accumulated charges and dissipated power produced during the different treatment conditions are presented in Table 2. Accumulated charges refer to the build-up of electrical charges within the PVA hydrogel during plasma treatment. The accumulated charges do not persist in the PVA hydrogel after the plasma is switched off; and therefore, these charges will not directly impact the hydrogel's biological performance. Rather, the importance of accumulated charges is to promote the electrochemical process involved in the activation of the PVA hydrogel with RONS during plasma treatment. The amount of RONS produced in the PVA hydrogel will influence the hydrogel's antibacterial activity. For the PVA treatments, maximum accumulated charges of 7.87±0.02 nC and dissipated power of 2.46±0.02 W were achieved with the PVA-GND-W condition.

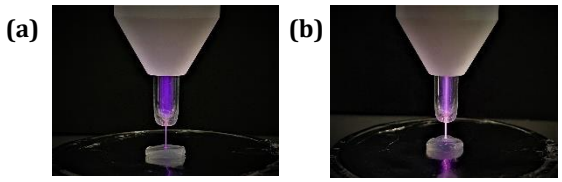

Figure 5. Photographs of the plasma jet during treatment of (a) PVA-FLT-W and (b) PVA-GND-W hydrogels.

The high energy state species produced by the plasma jet were studied through OES. The optical emission spectra of the plasma jet – PVA hydrogel interface or plasma jet – Al plate interface in the absence of the PVA hydrogel, are shown in Figure 6. All spectra show similar features from excited He (He*), nitrogen (N_2*), oxygen (O*), the ˙OH, nitric oxide gamma bands (NOγ), the nitrogen second positive system (N_2 SPS) and the nitrogen first negative system (N_2 FNS), which are all labeled in the graphs [47,48]. Many of these species are highly reactive with a short half-life and would be extinguished within the PVA hydrogel before it is applied to the target. However, these high-energy components of the plasma jet are responsible for triggering reactions in the gas phase that lead to the creation of downstream reactive species, including RONS [64], which are formed in the gas phase and in situ within the PVA hydrogel. For example, during plasma jet treatment of the PVA hydrogels, the ˙OH might be formed through collisional reactions with electrons, metastables, and by UV photolysis, as shown in Table 3 (Equations 7-11).

Table 3. Reaction pathway for the formation of the ˙OH in plasma jets [65–67].

How it occurs	Reactions	No.
Collision with electron	$e^- + H_2O \rightarrow H + OH + e^-.$	(7)
Collision with O_2 metastable	$e^- + O_2 \rightarrow O(^3P) + O(^1D) + e^-;$ $O(^1D) + H_2O \rightarrow 2^{\bullet}OH.$	(8)
Collision with N_2 metastable	$e^- + N_2 \rightarrow N_2(A^3\sum_u^+) + e^-;\ N_2(A^3\sum_u^+) + H_2O \rightarrow N_2 + {}^{\bullet}OH + {}^{\bullet}H.$	(9)
Collision with He metastable	$e^- + He \rightarrow He_m + e^-;\ He_m + H_2O \rightarrow He + {}^{\bullet}OH + {}^{\bullet}H.$	(10)
UV photolysis	$UV + H_2O \rightarrow H_2O^*; UV + H_2O^* \rightarrow H^+ + OH^-; OH^- \rightarrow e^- + {}^{\bullet}OH.$	(11)

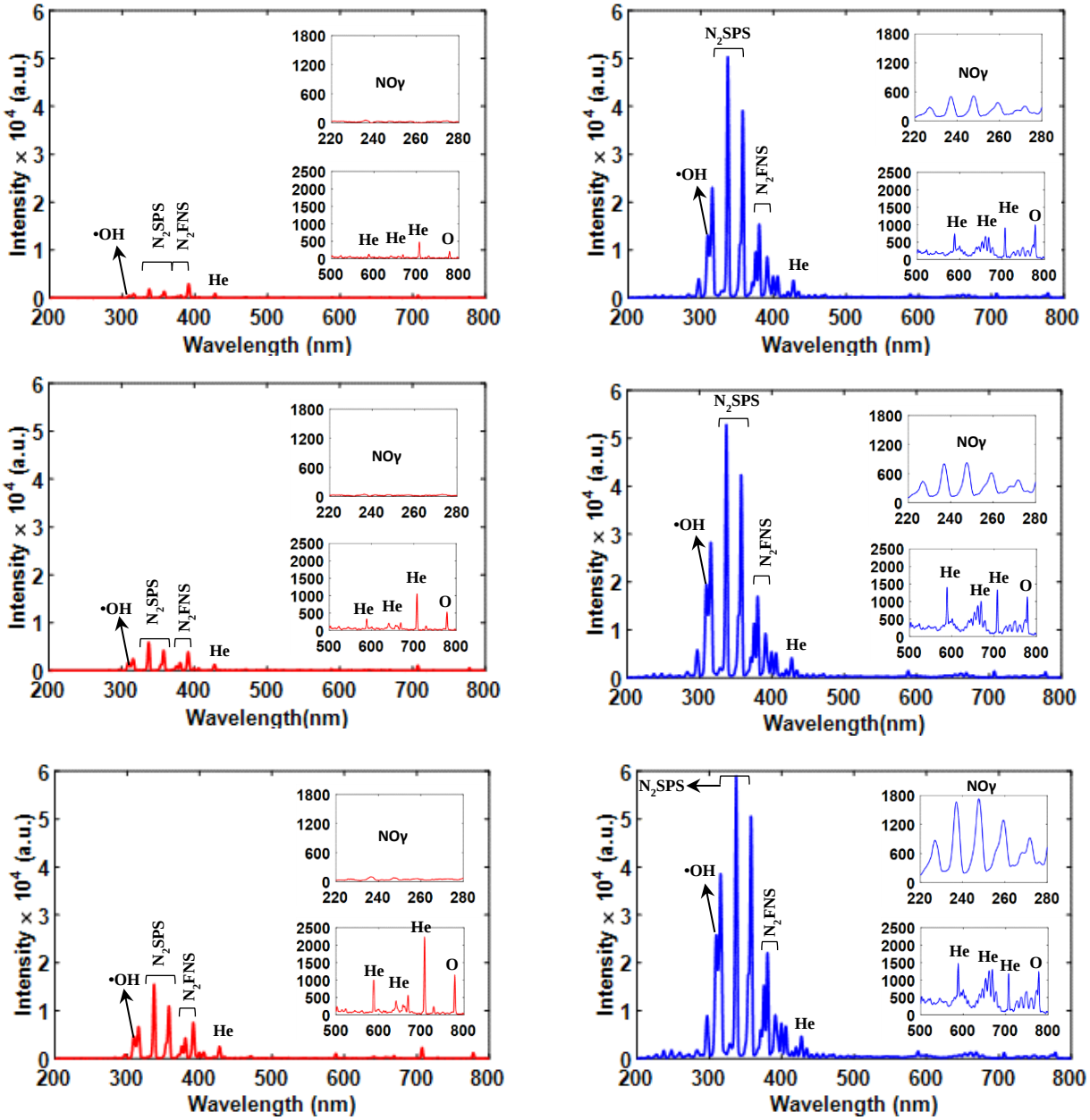

Figure 6. Optical emission spectra of at the plasma jet – Al plate interface or plasma jet – PVA hydrogel interface for (a) No PVA-FLT, (b) PVA-FLT, (c) PVA-FLT-W, (d) No PVA-GND, (e) PVA-GND, and (f) PVA-GND-W conditions. The graphs inset show magnified regions of the optical emission profile.

Recombination of the •OH molecules can subsequently produce H_2O_2 as shown in Equation 12.

$$^{\bullet}OH + {}^{\bullet}OH \rightarrow H_2O_2 \qquad (12)$$

Moreover, high energy oxygen and nitrogen atoms produced through electron dissociation reactions, shown in Equation 13-14, can produce various NO_x in the PVA hydrogel through the chemical reactions presented in Table 4 (Equation 15-17).

$$e^- + N_2 \rightarrow N + N + e^-. \quad (13)$$

$$e^- + O_2 \rightarrow O + O + e^-. \quad (14)$$

Table 4. Chemical reactions producing NO_x [68,69]

RNS	Reactions	No.
NO	$N + O_2 \rightarrow NO + O; N + {}^{\bullet}OH \rightarrow NO + {}^{\bullet}H; N + O \rightarrow NO.$	(15)
NO_2^-	$4NO + 2O_2 + 2H_2O \rightarrow NO_2^- + 4H^+.$	(16)
NO_3^-	$NO_2^- + H_2O_2 + H^+ \rightarrow NO_3^- + H_2O + H^+.$	(17)

Furthermore, the photons detected in the plasma jet between 236-380 nm have energies in the range of 5.25-3.27 eV, respectively, which is sufficient to dissociate water molecules through UV photolysis [51]. Grounding the plasma treatment system enhanced all the important components of the plasma jet required for promoting production of RONS (comparing Figure 7 (a), 7 (b) and 7 (c) to 7 (d), (e) and (f)). This was further enhanced through addition of the PVA hydrogel into the plasma treatment system (Figure 7 (b) and 7 (e)), and by hydrating the PVA hydrogel (Figure 7 (c) and 7 (f)). The reason for this is that grounding and hydrating the PVA hydrogel increases the discharge current, accumulated charges and dissipated power as discussed earlier. This also led to an increase in the photon energy density.

Table 5. Photon energy density at 309 nm, and plasma vibrational and rotational temperatures produced during different treatment conditions.[a]

Target conditions	Photon energy density at 309 nm [mJ/m^2]	Vibrational temperature [K]	Rotational temperature [K]
No PVA- FLT	0.04	3650	300
No PVA-GND	1.06	3850	300
PVA-FLT	0.23	3200	300
PVA-FLT-W	0.3	3400	300

PVA-GND	1	4200	300
PVA-GND-W	2.38	4400	300

[a] Vibrational and rotational temperatures are calculated from the fitted curves shown in Figure S7 of the supplementary material.

For example, the photon energy density at 309 nm corresponding to the emission from the $^{\bullet}OH$ (and important for producing H_2O_2 in the PVA hydrogel) increased from 0.3 mJ/m^2 for the PVA-FLT-W hydrogel treatment to 2.38 mJ/m^2 for the PVA-GND-W hydrogel treatment (Table 5). Table 5 also shows that the plasma vibrational temperature (T_v) was much higher than the plasma rotational temperature (T_r) for all treatment conditions, which is indicative of the non-equilibrium nature of the plasma jet. Without considering inelastic collisions between the electrons and molecules, the T_v approximately equals the plasma electron temperature (T_e)[53,70,71]. This means that grounding and hydrating the plasma jet also promoted production of high temperature electrons (maximum of 4400 K for PVA-GND-W in Table 5) important for producing RONS through electron-impact dissociation reactions as described in Equation 7-10. T_r remained low for all conditions. This is important because T_r can be considered the gas temperature because of the rapid rotational relaxation through inelastic collisions between molecules and atoms [72]. Therefore, the results show that T_e can be increased through grounding and hydrating the PVA hydrogel whilst avoiding physical damage to it through gas heating.

3.3.2. Chemical enhancement through hydration

As shown earlier in Figure 3, hydrating the PVA hydrogel increased the humidity at the plasma jet – PVA hydrogel interface. This promoted production of H_2O_2 but did not affect NO_2^- production. The conductivity of the air will increase with increasing humidity, and this was shown to slightly increase the accumulated charges and dissipated power in Figure 3 and Table 2; however, this was not as significant as the electrical enhancement achieved by grounding the PVA hydrogel. Since NO_2^- production closely correlates with dissipated power but not humidity, this can explain why humidity did not affect NO_2^- production. Lower energy of 4 eV is required to dissociate H_2O molecules as compared to 11 eV that is required for N_2 molecules to be dissociated [73]. However, increasing humidity did promote production of H_2O_2. This can only be partially explained by the slight increase in dissipated power during plasma jet treatment under high humidity. Rather, the increase in H_2O_2 production by

hydration was mainly attributed to chemical processes through reactions involving water (H_2O) molecules shown in Equation 7-12.

H_2O molecules have a major role in all the major physical and chemical processes responsible in forming H_2O_2 within the PVA hydrogel. The reason for this is that when H_2O becomes dissociated by plasma it will readily recombine to form H_2O_2 (Equation 12). In the He plasma jet treatment system used in this paper, H_2O can be dissociated when it collides with an electron (Equation 7), an O_2 metastable (Equation 8), a N_2 metastable (Equation 9), a He metastable (Equation 10), or through UV photolysis (Equation 11). These reactions lead to the generation of the $^{\bullet}OH$ or hydroxyl ion (^{-}OH).

Whilst these reactions can occur within the plasma core (i.e., within the silica tube of the plasma jet assembly) from H_2O supplied by impurities in the He gas supply and from residual water adsorbed to the gas tubing and inner wall of the silica tube, H_2O_2 can also be formed in the afterglow region (i.e., downstream of the plasma core) when the plasma jet mixes with the ambient air [48]. Therefore, mixing the effluent of the plasma jet with ambient air rich in H_2O molecules will promote H_2O_2 production. In addition, the H_2O molecules will also dilute the nitrogen molecules that can decrease the concentration of H_2O_2 through quenching reactions (Equations 6, and 17). Therefore, concurrently promoting reactions that produce H_2O_2 and limiting reactions that quench H_2O_2 significantly enhanced H_2O_2 production within the PVA hydrogel.

Additional hydration did not affect NO_2^- production. This is due to less dependency of NO_2^- production on air humidity (Equation 13-15) [47,48,60]. Rather, generation of NO_2^- is highly dependent on the interaction of the plasma effluent with the N_2 (78%) and O_2 (21%) molecules in the ambient air (Equation 9-10) than H_2O [48,60,74].

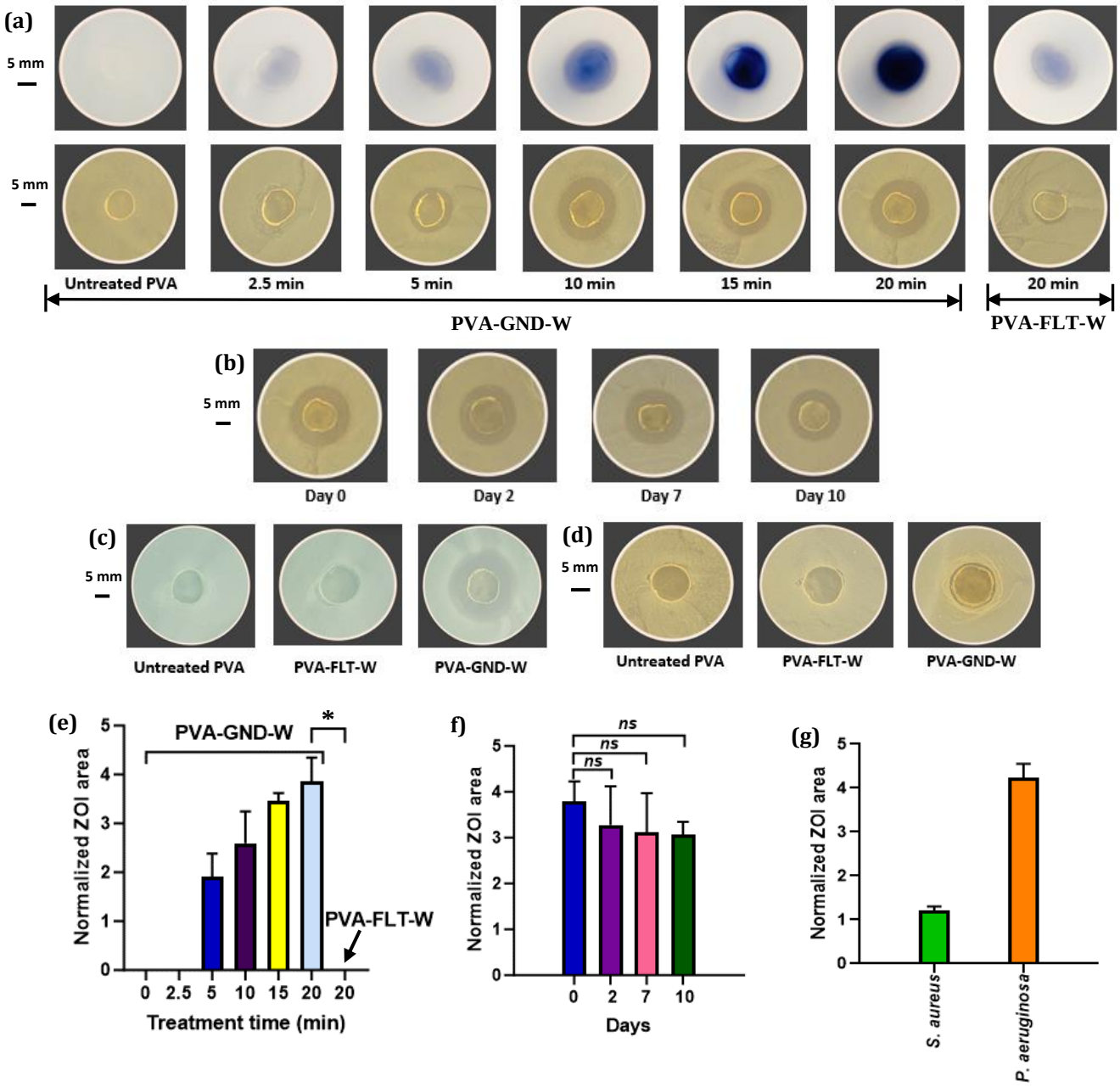

Figure 7. (a) Photographs of colour intensity (RONS transfer) produced in the agarose containing the by KI-starch RONS reporter dye (top row) and corresponding photographs of E. coli ZOI (bottom row) for different plasma treatment times of PVA-GND-W hydrogels and the PVA-FLT-W hydrogel plasma treated for 20 min; quantified ZOI is shown in (e) (n = 6). (b) photographs and (f) quantified E. coli ZOI produced by 20 min plasma treated PVA-GND-W hydrogels freshly prepared (day 0) and following storage for 2, 7 and 10 days (n = 3). Photographs of (c) P. aeruginosa and (d) S. aureus ZOI and (g) quantified ZOI for both bacteria produced by freshly prepared 20 min plasma treated PVA-GND-W hydrogels (n = 3). Photographs of the of the petri dishes with PVA hydrogel on top are shown in Figure S2 to S6

of the supplementary material. Data are presented as mean ± standard error of the mean (SEM). * $p < 0.0001$, ^{ns} $p > 0.05$ (Student t-test). ns = not significant.

3.4. Linking oxidation potential to antibacterial activity

The ability of the PVA hydrogels to oxidize the agarose-KI-starch film was first tested for PVA hydrogels that were grounded and hydrated during plasma treatment. It can be seen in Figure *7* (a) that increasing the plasma treatment time up to 20 min resulted in a darker purple colour formed in the agarose film, indicating a higher level of KI oxidation. The colour in the agarose film spread further than the diameter of the PVA hydrogel discs, which indicates the PAHT can be used to deliver RONS over a circumference spanning greater than 10 mm in diameter in this study. If required, larger area treatments can be accomplished using a bundle of plasma jets (a.k.a. multi plasma jets) [75,76]. This directly corresponded with an increase in ZOI (Figure 7 (a)). The PVA hydrogel that was kept at floating potential and hydrated during 20 min of plasma treatment produced a lighter purple colour in the agarose film (compared to the PVA hydrogel that was grounded and hydrated during the 20 min plasma treatment), which did not lead to a prominent ZOI of *E. coli*. Overall, the results indicate that transfer of oxidative molecules from the PVA hydrogel to the target closely correlates with bactericidal activity. The quantified ZOI in Figure 7 (e) shows that the bactericidal action of the PVA-GND-W hydrogels is enhanced by the plasma treatment time (i.e., the dose of the oxidative molecules), which is also supported by the increase in H_2O_2 release as shown in Figure 3 (g). In the PVA-FLT-W only 0.7 mM H_2O_2 is produced (from Figure 3 (g)), which did not correlate with inhibition of bacterial growth (Figure 7 (a), 7 (c)-(e)). In the PVA-GND-W this increases to 3.4 mM, which effectively reduced bacterial growth as seen by an increase in the ZOI (Figure 7 (a)-(g)).

The shelf-life of the PVA-GND-W hydrogels prepared using 20 min of plasma treatments (which had the highest antibacterial activity) were tested by storing them in a conventional freezer for 2, 7 and 10 days. These PVA hydrogels were subsequently defrosted and then used in an *E. coli* ZOI experiment. It can be seen in Figure 7 (b) that storage did not significantly impact upon the bactericidal activity with no significant change in the resultant ZOI compared to the freshly prepared (Day 0) plasma treated hydrogels. *P. aeruginosa*, and *S. aureus* are two commonly found pathogenic bacteria in skin wounds. Therefore, the ability of the 20 min plasma treated PVA-FLT-W and PVA-GND-W hydrogels to inhibit growth of these bacteria was compared to the untreated PVA hydrogel as a negative control. A measurable ZOI was only observed for the 20 min PVA-GND-W hydrogels in Figure 7 (c) and 7 (d) as shown in

Figure 7 (g). However, the result also shows that *S. aureus* displayed a lower ZOI compared to *P. aeruginosa* (Figure 7 (g)). This suggests that *S. aureus* is more resistant to the oxidative molecules released by the plasma treated PVA hydrogel. This result is also consistent with previous studies that shows *S. aureus* is more resistant to plasma and plasma activated liquid treatments compared to *P. aeruginosa* [77–79]. Loading the PVA hydrogel with higher concentrations of oxidative molecules might further improve its bactericidal efficacy; this was not investigated as it was not needed to obtain proof-of-principle in this study but might be needed in the future to optimize the antibacterial activity of the plasma treated PVA hydrogels against specific bacteria.

To be effective, the plasma treated PVA hydrogels do not necessarily need to directly kill all bacteria. In real patient treatment it is likely that the plasma activated hydrogels will also indirectly kill through immune cell activation. The reason for this is that plasma has previously been shown to activate defence mechanisms of macrophages and other factors associated with wound decontamination and healing [80–83]. This suggests that RONS and other molecules generated by plasma have a key role in the activation of the immune system, which is likely to improve the effect on wound decontamination and healing.

3.5. Skin cell biocompatibility

The influence of the RONS and molecules eluted from the plasma treated PVA-GND-W hydrogels into cell culture media on cell viability was assessed using HaCaT keratinocytes and HFF fibroblasts. Because the PVA hydrogels would have physically disrupted the adherence of the cells in the tissue culture wells, cell viability was measured indirectly using the cell media that had been incubated with the PVA hydrogels prior to application to the cells. Cell viability was measured 24 and 48 h following incubation of the cell media containing the eluted molecules with the cells. Figure 8 shows that the PVA-GND-W hydrogels significantly reduced the viability of HaCaT (Figure (8a)) and HFF fibroblast (Figure (8b)) cells. This is not unexpected because the PVA-GND-W hydrogels produced in this study released over 500 µM H_2O_2, which was cytotoxic to both cell types with <80% cell viability (Figure 8(a) and 8(b)). The cell viability response did not significantly differ from 24 h to 48 h, which indicates that the cytotoxicity is more of an immediate effect as opposed to cumulative.

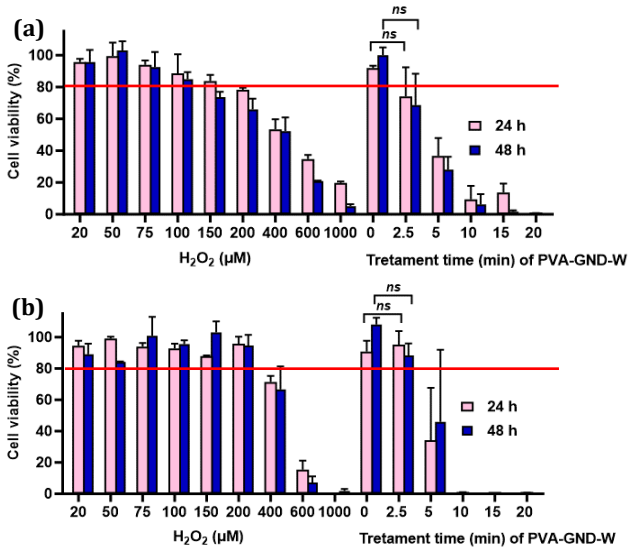

Figure 8. Effect of plasma treated PVA-GND-W hydrogels and standard H_2O_2 solutions on viability of (a) HaCaT keratinocyte and (b) HFF fibroblast cells (n = 4). Data are presented as mean ± SEM. $^{ns}p > 0.05$ (Student t-test). ns = not significant.

In the context of treatment of infected wounds, it is paramount to first eliminate infection before it becomes systemic, which can lead to life-threatening sepsis and osteomyelitis. Many antimicrobial agents are cytotoxic at high concentrations. What the plasma activated hydrogel system offers is the ability to modulate the dose of active agents (e.g., H_2O_2) to the phase of healing. For example, a 20 min plasma treated PVA-GND-W hydrogel might be needed initially to control infection. This treatment can then be later replaced with a non-cytotoxic 2.5 min plasma treated PVA-GND-W hydrogel dressing to prevent recurrence of infection and stimulate healing. However, in the context of developing a more effective and safer alternative antibacterial wound therapy to antibiotics and silver, it will be essential to test this new PAHT in living mammals to understand how physiological the environment impacts the treatment.

4. Conclusion and future directions

An electrochemical approach to enhance production of RONS in PAHT was investigated and characterized for controlling growth of common pathogenic bacteria found in wounds. Through electrochemical enhancement of the He plasma jet treatment system, an unprecedented 3.4 mM of H_2O_2 could be produced in the target PVA hydrogels. These dressings were highly effective at controlling growth of *E. coli* and *P. aeruginosa* and mildly effective against *S. aureus*. Validation of the new PAHT dressings *in vivo* will be required

next to ensure the technology is effective and safe for wound treatment. Nonetheless, the new technology does offer a promising alternative to existing treatments of antibiotics and silver dressings that will need to be replaced due to escalating problems of AMR and accumulative silver toxicity.

5. Acknowledgments

E.J.S. acknowledges the support from the Australian Research Council Future Fellowship No. FT190100263, and the National Health Medical Research Council Ideas Grant No. 2002510. We thank Professor Allison Cowin (UniSA) for providing the HaCaT and HFF cell lines. The authors wish to thank Professor Hiroshi Akatsuka at Tokyo Institute of Technology for providing a spectrum simulator of the N_2 second positive system.

6. References

(1) Franklin, H.; Rajan, M.; Tseng, C.-L.; Pogach, L.; Sinha, A.; Mph, M. Cost of Lower-Limb Amputation in U.S. Veterans with Diabetes Using Health Services Data in Fiscal Years 2004 and 2010. *J Rehabil Res Dev* **2014**, *51* (8), 1325–1330. https://doi.org/10.1682/JRRD.2013.11.0249.

(2) Roope, L. S. J.; Smith, R. D.; Pouwels, K. B.; Buchanan, J.; Abel, L.; Eibich, P.; Butler, C. C.; Tan, P. S.; Walker, A. S.; Robotham, J. V.; Wordsworth, S. The Challenge of Antimicrobial Resistance: What Economics Can Contribute. *Science* **2019**, *364* (6435), eaau4679. https://doi.org/10.1126/science.aau4679.

(3) Monahan, C.; Harris, S.; Morris, D.; Cummins, E. A Comparative Risk Ranking of Antibiotic Pollution from Human and Veterinary Antibiotic Usage – An Irish Case Study. *Science of The Total Environment* **2022**, *826*, 154008. https://doi.org/10.1016/j.scitotenv.2022.154008.

(4) Topp, E.; Larsson, D. G. J.; Miller, D. N.; Van Den Eede, C.; Virta, M. P. J. Antimicrobial Resistance and the Environment: Assessment of Advances, Gaps and Recommendations for Agriculture, Aquaculture and Pharmaceutical Manufacturing. *FEMS Microbiology Ecology* **2018**, *94* (3). https://doi.org/10.1093/femsec/fix185.

(5) Weller, C.; Weller, C.; Team, V. Interactive Dressings and Their Role in Moist Wound Management. In *Advanced Textiles for Wound Care*; Elsevier, 2019; pp 105–134. https://doi.org/10.1016/B978-0-08-102192-7.00004-7.

(6) Eaglstein, W. H. Moist Wound Healing with Occlusive Dressings: A Clinical Focus. *Dermatologic Surgery* **2001**, *27* (2), 175–182. https://doi.org/10.1046/j.1524-4725.2001.00299.x.

(7) Brölmann, F. E.; Eskes, A. M.; Goslings, J. C.; Niessen, F. B.; de Bree, R.; Vahl, A. C.; Pierik, E. G.; Vermeulen, H.; Ubbink, D. T. Randomized Clinical Trial of Donor-Site Wound Dressings after Split-Skin Grafting. *British Journal of Surgery* **2013**, *100* (5), 619–627. https://doi.org/10.1002/bjs.9045.

(8) Draelos, Z. D.; Rizer, R. L.; Trookman, N. S. A Comparison of Postprocedural Wound Care Treatments: Do Antibiotic-Based Ointments Improve Outcomes? *Journal of the American Academy of Dermatology* **2011**, *64* (3), S23–S29. https://doi.org/10.1016/j.jaad.2010.11.010.

(9) Kavitha, K. V. Choice of Wound Care in Diabetic Foot Ulcer: A Practical Approach. *WJD* **2014**, *5* (4), 546. https://doi.org/10.4239/wjd.v5.i4.546.

(10) Singh, A.; Halder, S.; Chumber, S.; Misra, M. C.; Sharma, L. K.; Srivastava, A.; Menon, G. R. Meta-Analysis of Randomized Controlled Trials on Hydrocolloid Occlusive Dressing Versus Conventional Gauze Dressing in the Healing of Chronic Wounds. *Asian Journal of Surgery* **2004**, *27* (4), 326–332. https://doi.org/10.1016/S1015-9584(09)60061-0.

(11) Bayat, A.; Ramaiah, R.; Bhananker, S. M. Analgesia and Sedation for Children Undergoing Burn Wound Care. Expert Review of Neurotherapeutics **2010**, 10 (11), 1747–1759. https://doi.org/10.1586/ern.10.158.

(12) Mirpour, S.; Fathollah, S.; Mansouri, P.; Larijani, B.; Ghoranneviss, M.; Mohajeri Tehrani, M.; Amini, M. R. Cold Atmospheric Plasma as an Effective Method to Treat Diabetic Foot Ulcers: A Randomized Clinical Trial. *Sci Rep* **2020**, *10* (1), 10440. https://doi.org/10.1038/s41598-020-67232-x.

(13) Stratmann, B.; Costea, T.-C.; Nolte, C.; Hiller, J.; Schmidt, J.; Reindel, J.; Masur, K.; Motz, W.; Timm, J.; Kerner, W.; Tschoepe, D. Effect of Cold Atmospheric Plasma Therapy vs Standard Therapy Placebo on Wound Healing in Patients With Diabetic Foot Ulcers: A Randomized Clinical Trial. *JAMA Netw Open* **2020**, *3* (7), e2010411. https://doi.org/10.1001/jamanetworkopen.2020.10411.

(14) Rutkowski, R.; Daeschlein, G.; Von Woedtke, T.; Smeets, R.; Gosau, M.; Metelmann, H.-R. Long-Term Risk Assessment for Medical Application of Cold Atmospheric Pressure Plasma. *Diagnostics* **2020**, *10* (4), 210. https://doi.org/10.3390/diagnostics10040210.

(15) Sabrin, S.; Karmokar, D. K.; Karmakar, N. C.; Hong, S.-H.; Habibullah, H.; Szili, E. J. Opportunities of Electronic and Optical Sensors in Autonomous Medical Plasma Technologies. *ACS Sens.* **2023**, *8* (3), 974–993. https://doi.org/10.1021/acssensors.2c02579.

(16) Wen, Q.; Liu, D.; Wang, X.; Zhang, Y.; Fang, S.; Qiu, X.; Chen, Q. Effects of Ozone for Treating Chronically Refractory Wounds and Ulcers: A Protocol for Systematic Review and Meta-Analysis of Randomized Clinical Trials. *Medicine* **2020**, *99* (22), e20457. https://doi.org/10.1097/MD.0000000000020457.

(17) Gorbanev, Y.; Privat-Maldonado, A.; Bogaerts, A. Analysis of Short-Lived Reactive Species in Plasma–Air–Water Systems: The Dos and the Do Nots. *Anal. Chem.* **2018**, *90* (22), 13151–13158. https://doi.org/10.1021/acs.analchem.8b03336.

(18) Loo, A. E. K.; Wong, Y. T.; Ho, R.; Wasser, M.; Du, T.; Ng, W. T.; Halliwell, B. Effects of Hydrogen Peroxide on Wound Healing in Mice in Relation to Oxidative Damage. *PLoS ONE* **2012**, *7* (11), e49215. https://doi.org/10.1371/journal.pone.0049215.

(19) Uhm, H. S. Generation of Various Radicals in Nitrogen Plasma and Their Behavior in Media. *Physics of Plasmas* **2015**, *22* (12), 123506. https://doi.org/10.1063/1.4936796.

(20) Khlyustova, A.; Labay, C.; Machala, Z.; Ginebra, M.-P.; Canal, C. Important Parameters in Plasma Jets for the Production of RONS in Liquids for Plasma Medicine: A Brief Review. *Front. Chem. Sci. Eng.* **2019**, *13* (2), 238–252. https://doi.org/10.1007/s11705-019-1801-8.

(21) Ikawa, S.; Tani, A.; Nakashima, Y.; Kitano, K. Physicochemical Properties of Bactericidal Plasma-Treated Water. *J. Phys. D: Appl. Phys.* **2016**, *49* (42), 425401. https://doi.org/10.1088/0022-3727/49/42/425401.

(22) Gaur, N.; Patenall, B. L.; Ghimire, B.; Thet, N. T.; Gardiner, J. E.; Le Doare, K. E.; Ramage, G.; Short, B.; Heylen, R. A.; Williams, C.; Short, R. D.; Jenkins, T. A. Cold Atmospheric Plasma-Activated Composite Hydrogel for an Enhanced and On-Demand Delivery of Antimicrobials. *ACS Appl. Mater. Interfaces* **2023**, *15* (16), 19989–19996. https://doi.org/10.1021/acsami.3c01208.

(23) Naïtali, M.; Kamgang-Youbi, G.; Herry, J.-M.; Bellon-Fontaine, M.-N.; Brisset, J.-L. Combined Effects of Long-Living Chemical Species during Microbial Inactivation Using Atmospheric Plasma-Treated Water.

Applied and Environmental Microbiology **2010**, *76* (22), 7662–7664. https://doi.org/10.1128/AEM.01615-10.

(24) Liu, Z.; Zheng, Y.; Dang, J.; Zhang, J.; Dong, F.; Wang, K.; Zhang, J. A Novel Antifungal Plasma-Activated Hydrogel. *ACS Appl. Mater. Interfaces* **2019**, *11* (26), 22941–22949. https://doi.org/10.1021/acsami.9b04700.

(25) Zhai, S.; Xu, M.; Li, Q.; Guo, K.; Chen, H.; Kong, M. G.; Xia, Y. Successful Treatment of Vitiligo with Cold Atmospheric Plasma–Activated Hydrogel. *Journal of Investigative Dermatology* **2021**, *141* (11), 2710-2719.e6. https://doi.org/10.1016/j.jid.2021.04.019.

(26) Labay, C.; Roldán, M.; Tampieri, F.; Stancampiano, A.; Bocanegra, P. E.; Ginebra, M.-P.; Canal, C. Enhanced Generation of Reactive Species by Cold Plasma in Gelatin Solutions for Selective Cancer Cell Death. *ACS Appl. Mater. Interfaces* **2020**, *12* (42), 47256–47269. https://doi.org/10.1021/acsami.0c12930.

(27) Labay, C.; Hamouda, I.; Tampieri, F.; Ginebra, M.-P.; Canal, C. Production of Reactive Species in Alginate Hydrogels for Cold Atmospheric Plasma-Based Therapies. *Sci Rep* **2019**, *9* (1), 16160. https://doi.org/10.1038/s41598-019-52673-w.

(28) LaRiviere, C. A.; Goldin, A. B.; Avansino, J. Silver Toxicity With the Use of Silver-Impregnated Dressing and Wound Vacuum-Assisted Closure in an Immunocompromised Patient. *J Am Col Certif Wound Spec* **2011**, *3* (1), 8–12. https://doi.org/10.1016/j.jcws.2011.05.002.

(29) Haidari, H.; Garg, S.; Vasilev, K.; Kopecki, Z.; Cowin, A. Silver-Based Wound Dressings: Current Issues and Future Developments for Treating Bacterial Infections. *WPR* **2020**, *28* (4). https://doi.org/10.33235/wpr.28.4.173-180.

(30) Branda, S. S.; Chu, F.; Kearns, D. B.; Losick, R.; Kolter, R. A Major Protein Component of the Bacillus Subtilis Biofilm Matrix. *Mol Microbiol* **2006**, *59* (4), 1229–1238. https://doi.org/10.1111/j.1365-2958.2005.05020.x.

(31) Arora, V. Cold Atmospheric Plasma (CAP) In Dentistry. *Dentistry* **2013**, *04* (01). https://doi.org/10.4172/2161-1122.1000189.

(32) Pandit, S.; Vrss, M.; Helgadottir, S. H.; Westerlund, F.; Mijakovic, I. Combination of Cold Atmospheric Plasma and Vitamin C Effectively Disrupts Bacterial Biofilms. *Clin Microbiol* **2017**, *06* (03). https://doi.org/10.4172/2327-5073.1000283.

(33) Barnes, A. M. T.; Ballering, K. S.; Leibman, R. S.; Wells, C. L.; Dunny, G. M. Enterococcus Faecalis Produces Abundant Extracellular Structures Containing DNA in the Absence of Cell Lysis during Early Biofilm Formation. *mBio* **2012**, *3* (4), e00193-12. https://doi.org/10.1128/mBio.00193-12.

(34) Mai-Prochnow, A.; Bradbury, M.; Ostrikov, K.; Murphy, A. B. Pseudomonas Aeruginosa Biofilm Response and Resistance to Cold Atmospheric Pressure Plasma Is Linked to the Redox-Active Molecule Phenazine. *PLoS ONE* **2015**, *10* (6), e0130373. https://doi.org/10.1371/journal.pone.0130373.

(35) Chen, J.; Wang, Z.; Sun, J.; Zhou, R.; Guo, L.; Zhang, H.; Liu, D.; Rong, M.; Ostrikov, K. (Ken). Plasma-Activated Hydrogels for Microbial Disinfection. *Advanced Science* **2023**, *10* (14), 2207407. https://doi.org/10.1002/advs.202207407.

(36) Omran, A. V.; Busco, G.; Dozias, S.; Grillon, C.; Pouvesle, J.-M.; Robert, E. Distribution and Penetration of Reactive Oxygen and Nitrogen Species through a Tissue Phantom after Plasma Gun Treatment.

(37) Ki, S. H.; Masur, K.; Baik, K. Y.; Choi, E. H. UV Absorption Spectroscopy for the Diffusion of Plasma-Generated Reactive Species through a Skin Model. *Applied Sciences* **2021**, *11* (17), 7958. https://doi.org/10.3390/app11177958.

(38) Wilkins, R. G.; Unverdorben, M. Wound Cleaning and Wound Healing: A Concise Review. **2013**, *26* (4).

(39) White, R. J.; Cooper, R.; Kingsley, A. Wound Colonization and Infection: The Role of Topical Antimicrobials. *Br J Nurs* **2001**, *10* (9), 563–578. https://doi.org/10.12968/bjon.2001.10.9.9387.

(40) Fang, H.; Wang, J.; Li, L.; Xu, L.; Wu, Y.; Wang, Y.; Fei, X.; Tian, J.; Li, Y. A Novel High-Strength Poly(Ionic Liquid)/PVA Hydrogel Dressing for Antibacterial Applications. *Chemical Engineering Journal* **2019**, *365*, 153–164. https://doi.org/10.1016/j.cej.2019.02.030.

(41) Alipoori, S.; Mazinani, S.; Aboutalebi, S. H.; Sharif, F. Review of PVA-Based Gel Polymer Electrolytes in Flexible Solid-State Supercapacitors: Opportunities and Challenges. *Journal of Energy Storage* **2020**, *27*, 101072. https://doi.org/10.1016/j.est.2019.101072.

(42) Ito, Y.; Urabe, K.; Takano, N.; Tachibana, K. High Speed Deposition of SiO_2 Films with Plasma Jet Based on Capillary Dielectric Barrier Discharge at Atmospheric Pressure. *Appl. Phys. Express* **2008**, *1*, 067009. https://doi.org/10.1143/APEX.1.067009.

(43) Oh, J.-S.; Szili, E. J.; Gaur, N.; Hong, S.-H.; Furuta, H.; Short, R. D.; Hatta, A. In-Situ UV Absorption Spectroscopy for Monitoring Transport of Plasma Reactive Species through Agarose as Surrogate for Tissue. *J. Photopol. Sci. Technol.* **2015**, *28* (3), 439–444. https://doi.org/10.2494/photopolymer.28.439.

(44) Gaur, N.; Kurita, H.; Oh, J.-S.; Miyachika, S.; Ito, M.; Mizuno, A.; Cowin, A. J.; Allinson, S.; Short, R. D.; Szili, E. J. On Cold Atmospheric-Pressure Plasma Jet Induced DNA Damage in Cells. *J. Phys. D: Appl. Phys.* **2021**, *54* (3), 035203. https://doi.org/10.1088/1361-6463/abb8ab.

(45) Szili, E. J.; Oh, J.-S.; Hong, S.-H.; Hatta, A.; Short, R. D. Probing the Transport of Plasma-Generated RONS in an Agarose Target as Surrogate for Real Tissue: Dependency on Time, Distance and Material Composition. *J. Phys. D: Appl. Phys.* **2015**, *48* (20), 202001. https://doi.org/10.1088/0022-3727/48/20/202001.

(46) Oh, J.-S.; Szili, E. J.; Gaur, N.; Hong, S.-H.; Furuta, H.; Kurita, H.; Mizuno, A.; Hatta, A.; Short, R. D. How to Assess the Plasma Delivery of RONS into Tissue Fluid and Tissue. *J. Phys. D: Appl. Phys.* **2016**, *49* (30), 304005. https://doi.org/10.1088/0022-3727/49/30/304005.

(47) Ghimire, B.; Patenall, B. L.; Szili, E. J.; Gaur, N.; Lamichhane, P.; Thet, N. T.; Trivedi, D.; Jenkins, A. T. A.; Short, R. D. The Influence of a Second Ground Electrode on Hydrogen Peroxide Production from an Atmospheric Pressure Argon Plasma Jet and Correlation to Antibacterial Efficacy and Mammalian Cell Cytotoxicity. *J. Phys. D: Appl. Phys.* **2022**, *55* (12), 125207. https://doi.org/10.1088/1361-6463/ac43d9.

(48) Ghimire, B.; Szili, E. J.; Patenall, B. L.; Lamichhane, P.; Gaur, N.; Robson, A. J.; Trivedi, D.; Thet, N. T.; Jenkins, A. T. A.; Choi, E. H.; Short, R. D. Enhancement of Hydrogen Peroxide Production from an Atmospheric Pressure Argon Plasma Jet and Implications to the Antibacterial Activity of Plasma Activated Water. *Plasma Sources Sci. Technol.* **2021**, *30* (3), 035009. https://doi.org/10.1088/1361-6595/abe0c9.

(49) Szili, E. J.; Bradley, J. W.; Short, R. D. A 'Tissue Model' to Study the Plasma Delivery of Reactive Oxygen Species. *J. Phys. D: Appl. Phys.* **2014**, *47* (15), 152002. https://doi.org/10.1088/0022-3727/47/15/152002.

(50) Ghimire, B.; Patenall, B. L.; Szili, E. J.; Gaur, N.; Lamichhane, P.; Thet, N. T.; Trivedi, D.; Jenkins, A. T. A.; Short, R. D. The Influence of a Second Ground Electrode on Hydrogen Peroxide Production from an Atmospheric Pressure Argon Plasma Jet and Correlation to Antibacterial Efficacy and Mammalian Cell Cytotoxicity. *J. Phys. D: Appl. Phys.* **2022**, *55* (12), 125207. https://doi.org/10.1088/1361-6463/ac43d9.

(51) Ghimire, B.; Szili, E. J.; Lamichhane, P.; Short, R. D.; Lim, J. S.; Attri, P.; Masur, K.; Weltmann, K.-D.; Hong, S.-H.; Choi, E. H. The Role of UV Photolysis and Molecular Transport in the Generation of Reactive Species in a Tissue Model with a Cold Atmospheric Pressure Plasma Jet. *Appl. Phys. Lett.* **2019**, *114* (9), 093701. https://doi.org/10.1063/1.5086522.

(52) Oh; Szili; Hatta; Ito; Shirafuji. Tailoring the Chemistry of Plasma-Activated Water Using a DC-Pulse-Driven Non-Thermal Atmospheric-Pressure Helium Plasma Jet. *Plasma* **2019**, *2* (2), 127–137. https://doi.org/10.3390/plasma2020010.

(53) Szili, E. J.; Oh, J.-S.; Fukuhara, H.; Bhatia, R.; Gaur, N.; Nguyen, C. K.; Hong, S.-H.; Ito, S.; Ogawa, K.; Kawada, C.; Shuin, T.; Tsuda, M.; Furihata, M.; Kurabayashi, A.; Furuta, H.; Ito, M.; Inoue, K.; Hatta, A.; Short, R. D. Modelling the Helium Plasma Jet Delivery of Reactive Species into a 3D Cancer Tumour. *Plasma Sources Sci. Technol.* **2017**, *27* (1), 014001. https://doi.org/10.1088/1361-6595/aa9b3b.

(54) Szili, E. J.; Hong, S.-H.; Oh, J.-S.; Gaur, N.; Short, R. D. Tracking the Penetration of Plasma Reactive Species in Tissue Models. *Trends in Biotechnology* **2018**, *36* (6), 594–602. https://doi.org/10.1016/j.tibtech.2017.07.012.

(55) Thulliez, M.; Bastin, O.; Remy, A.; Nonclercq, A.; Devière, J.; Delchambre, A.; Reniers, F. Effect of Gas Flow on a Helium/Oxygen Endoscopic Plasma Jet. *J. Phys. D: Appl. Phys.* **2022**, *55* (41), 415202. https://doi.org/10.1088/1361-6463/ac7f03.

(56) Vasani, R. B.; Szili, E. J.; Rajeev, G.; Voelcker, N. H. On-Demand Antimicrobial Treatment with Antibiotic-Loaded Porous Silicon Capped with a pH-Responsive Dual Plasma Polymer Barrier. *Chem. Asian J.* **2017**, *12* (13), 1605–1614. https://doi.org/10.1002/asia.201700427.

(57) EUCAST Disk Diffusion Method for Antimicrobial Susceptibility Testing. **2021,** Version 9.0. http://www.eucast.org/.

(58) Hao, Z.; Ji, S.; Liu, H.; Song, Y. Effect of the Grounded Electrode on Cold Ar Atmospheric Pressure Plasma Jet Generated With a Simple DBD Configuration. *IEEE Trans. Plasma Sci.* **2014**, *42* (3), 824–832. https://doi.org/10.1109/TPS.2014.2303653.

(59) Mohamed, A.-A. H.; Aljuhani, M. M.; Almarashi, J. Q. M.; Alhazime, A. A. The Effect of a Second Grounded Electrode on the Atmospheric Pressure Argon Plasma Jet. *Plasma Res. Express* **2020**, *2* (1), 015011. https://doi.org/10.1088/2516-1067/ab7b36.

(60) Khlyustova, A.; Labay, C.; Machala, Z.; Ginebra, M.-P.; Canal, C. Important Parameters in Plasma Jets for the Production of RONS in Liquids for Plasma Medicine: A Brief Review. *Front. Chem. Sci. Eng.* **2019**, *13* (2), 238–252. https://doi.org/10.1007/s11705-019-1801-8.

(61) Abdelaziz, A.; Abdel-Salam, M.; Hashim, A.; Hammad, G.; Kim, H.-H. Development and characterization of surface dielectric barrier discharge-based reactor for ozone production. *Assiut University Journal of Multidisciplinary Scientific Research* **2020**, *49* (1), 17–34. https://doi.org/10.21608/aunj.2020.220860.

(62) Zito, J.; Arnold, D.; Durscher, R.; Roy, S. Investigation of Impedance Characteristics and Power Delivery for Dielectric Barrier Discharge Plasma Actuators. In *48th AIAA Aerospace Sciences Meeting Including the New Horizons Forum and Aerospace Exposition*; American Institute of Aeronautics and Astronautics: Orlando, Florida, 2010. https://doi.org/10.2514/6.2010-964.

(63) Neretti; Ricco. Self-Tuning High-Voltage and High-Frequency Sinusoidal Power Supply for Dielectric Barrier Discharge Plasma Generation. *Electronics* **2019**, *8* (10), 1137. https://doi.org/10.3390/electronics8101137.

(64) Lu, X.; Naidis, G. V.; Laroussi, M.; Reuter, S.; Graves, D. B.; Ostrikov, K. Reactive Species in Non-Equilibrium Atmospheric-Pressure Plasmas: Generation, Transport, and Biological Effects. *Physics Reports* **2016**, *630*, 1–84. https://doi.org/10.1016/j.physrep.2016.03.003.

(65) Chen, Z.; Liu, D.; Chen, C.; Xu, D.; Liu, Z.; Xia, W.; Rong, M.; Kong, M. G. Analysis of the Production Mechanism of H_2O_2 in Water Treated by Helium DC Plasma Jets. *J. Phys. D: Appl. Phys.* **2018**, *51* (32), 325201. https://doi.org/10.1088/1361-6463/aad0eb.

(66) Jiang, Y.; Wang, Y.; Cong, S.; Zhang, J.; Wang, D. Effects of Nitrogen Impurity on the Atmospheric Pressure Helium Plasma Jets Exposed to a Nitrogen Environment. *Physics of Plasmas* **2020**, *27* (10), 103511. https://doi.org/10.1063/5.0020468.

(67) Liu, X. Y.; Pei, X. K.; Ostrikov, K.; Lu, X. P.; Liu, D. W. The Production Mechanisms of OH Radicals in a Pulsed Direct Current Plasma Jet. *Physics of Plasmas* **2014**, *21* (9), 093513. https://doi.org/10.1063/1.4895496.

(68) Chen, Z.; Liu, D.; Xu, H.; Xia, W.; Liu, Z.; Xu, D.; Rong, M.; Kong, M. G. Decoupling Analysis of the Production Mechanism of Aqueous Reactive Species Induced by a Helium Plasma Jet. *Plasma Sources Sci. Technol.* **2019**, *28* (2), 025001. https://doi.org/10.1088/1361-6595/ab006b.

(69) Ghimire, B.; Szili, E. J.; Patenall, B. L.; Lamichhane, P.; Gaur, N.; Robson, A. J.; Trivedi, D.; Thet, N. T.; Jenkins, A. T. A.; Choi, E. H.; Short, R. D. Enhancement of Hydrogen Peroxide Production from an Atmospheric Pressure Argon Plasma Jet and Implications to the Antibacterial Activity of Plasma Activated Water. *Plasma Sources Sci. Technol.* **2021**, *30* (3), 035009. https://doi.org/10.1088/1361-6595/abe0c9.

(70) Kurihara, J.; Iwagami, N. N2 Temperature of Vibration Instrument for Sounding Rocket Observation in the Lower Thermosphere.

(71) Ioup, J. W.; Russek, A. Vibrational-Rotational Excitation in Atom-Diatomic-Molecule Collisions. *Phys. Rev. A* **1973**, *8* (6), 2898–2914. https://doi.org/10.1103/PhysRevA.8.2898.

(72) Bruggeman, P. J.; Sadeghi, N.; Schram, D. C.; Linss, V. Gas Temperature Determination from Rotational Lines in Non-Equilibrium Plasmas: A Review. *Plasma Sources Science and Technology* **2014**, *23* (2), 023001. https://doi.org/10.1088/0963-0252/23/2/023001.

(73) Ghimire, B.; Sornsakdanuphap, J.; Hong, Y. J.; Uhm, H. S.; Weltmann, K.-D.; Choi, E. H. The Effect of the Gap Distance between an Atmospheric-Pressure Plasma Jet Nozzle and Liquid Surface on OH and N2 Species Concentrations. *Physics of Plasmas* **2017**, *24* (7), 073502. https://doi.org/10.1063/1.4989735.

(74) Reuter, S.; Tresp, H.; Wende, K.; Hammer, M. U.; Winter, J.; Masur, K.; Schmidt-Bleker, A.; Weltmann, K.-D. From RONS to ROS: Tailoring Plasma Jet Treatment of Skin Cells. *IEEE Trans. Plasma Sci.* **2012**, *40* (11), 2986–2993. https://doi.org/10.1109/TPS.2012.2207130.

(75) Maho, T.; Binois, R.; Brulé-Morabito, F.; Demasure, M.; Douat, C.; Dozias, S.; Escot Bocanegra, P.; Goard, I.; Hocqueloux, L.; Le Helloco, C.; Orel, I.; Pouvesle, J.-M.; Prazuck, T.; Stancampiano, A.; Tocaben, C.; Robert, E. Anti-Bacterial Action of Plasma Multi-Jets in the Context of Chronic Wound Healing. *Applied Sciences* **2021**, *11* (20), 9598. https://doi.org/10.3390/app11209598.

(76) Ghimire, B.; Szili, E. J.; Short, R. D. A Conical Assembly of Six Plasma Jets for Biomedical Applications. *Applied Physics Letters* **2022**, *121* (8), 084102. https://doi.org/10.1063/5.0104481.

(77) Szili, E. J.; Ghimire, B.; Patenall, B. L.; Rohaim, M.; Mistry, D.; Fellows, A.; Munir, M.; Jenkins, A. T. A.; Short, R. D. On-Demand Cold Plasma Activation of Acetyl Donors for Bacteria and Virus Decontamination. *Applied Physics Letters* **2021**, *119* (5), 054104. https://doi.org/10.1063/5.0062787.

(78) Szili, E. J.; Patenall, B. L.; Fellows, A.; Mistry, D.; Jenkins, A. T. A.; Short, R. D.; Ghimire, B. On Plasma Activated Acetyl Donors: Comparing the Antibacterial Efficacy of Tetraacetylethylenediamine and Pentaacetate Glucose. *Plasma* **2022**, *5* (4), 423–435. https://doi.org/10.3390/plasma5040031.

(79) Baz, A.; Bakri, A.; Butcher, M.; Short, B.; Ghimire, B.; Gaur, N.; Jenkins, T.; Short, R. D.; Riggio, M.; Williams, C.; Ramage, G.; Brown, J. L. Staphylococcus Aureus Strains Exhibit Heterogenous Tolerance to Direct Cold Atmospheric Plasma Therapy. *Biofilm* **2023**, *5*, 100123. https://doi.org/10.1016/j.bioflm.2023.100123.

(80) Duchesne, C.; Banzet, S.; Lataillade, J.; Rousseau, A.; Frescaline, N. Cold Atmospheric Plasma Modulates Endothelial Nitric Oxide Synthase Signalling and Enhances Burn Wound Neovascularisation. *The Journal of Pathology* **2019**, *249* (3), 368–380. https://doi.org/10.1002/path.5323.

(81) Arndt, S.; Unger, P.; Wacker, E.; Shimizu, T.; Heinlin, J.; Li, Y.-F.; Thomas, H. M.; Morfill, G. E.; Zimmermann, J. L.; Bosserhoff, A.-K.; Karrer, S. Cold Atmospheric Plasma (CAP) Changes Gene Expression of Key Molecules of the Wound Healing Machinery and Improves Wound Healing In Vitro and In Vivo. *PLoS ONE* **2013**, *8* (11), e79325. https://doi.org/10.1371/journal.pone.0079325.

(82) Lee, Y.; Ricky, S.; Lim, T. H.; Kim, H.; Lee, E. J.; Song, Y.; Lee, S.; Jang, Y. An Atmospheric Plasma Jet Induces Expression of Wound Healing Genes in Progressive Burn Wounds in a Comb Burn Rat Model: A Pilot Study. *Journal of Burn Care & Research* **2023**, *44* (3), 685–692. https://doi.org/10.1093/jbcr/irab005.

(83) Dang, C. P.; Weawseetong, S.; Charoensappakit, A.; Sae-Khow, K.; Thong-Aram, D.; Leelahavanichkul, A. Non-Thermal Atmospheric Pressure Argon-Sourced Plasma Flux Promotes Wound Healing of Burn Wounds and Burn Wounds with Infection in Mice through the Anti-Inflammatory Macrophages. *Applied Sciences* **2021**, *11* (12), 5343. https://doi.org/10.3390/app11125343.

Supporting Information

Supporting Information is available from the Wiley Online Library or from the author.

Table of Contents

The table of contents entry: An electrochemical approach is investigated to enhance the antimicrobial action of plasma activated hydrogel therapy (PAHT). The paper explores the electrochemical mechanisms that underpin increased H_2O_2 production in PAHT and how this enhances PAHT's antibacterial efficacy against prevalent wound pathogens. Electrochemically enhanced PAHT is shown to be a promising new wound dressing to overcome escalating challenges in antimicrobial resistance.

Sumyea Sabrin*, Sung-Ha Hong , Sushil Kumar KC , Jun-Seok Oh, Ainslie L.K. Derrick-Roberts , Debabrata K. Karmokar , Habibullah Habibullah , Robert D. Short, Bhagirath Ghimire, Robert Fitridge , Endre J. Szili*

Electrochemically Enhanced Antimicrobial Action of Plasma Activated Poly(vinyl alcohol) Hydrogel Dressings

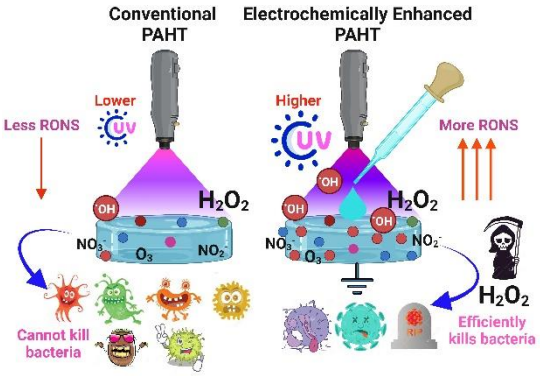

Supporting Information

Electrochemically Enhanced Antimicrobial Action of Plasma Activated Poly(vinyl alcohol) Hydrogel Dressings

Sumyea Sabrin, Sung-Ha Hong , Sushil Kumar KC , Jun-Seok Oh, Ainslie L.K. Derrick-Roberts , Debabrata K. Karmokar , Habibullah Habibullah , Robert D. Short, Bhagirath Ghimire, Robert Fitridge , Endre J. Szili**

TABLE OF FIGURES

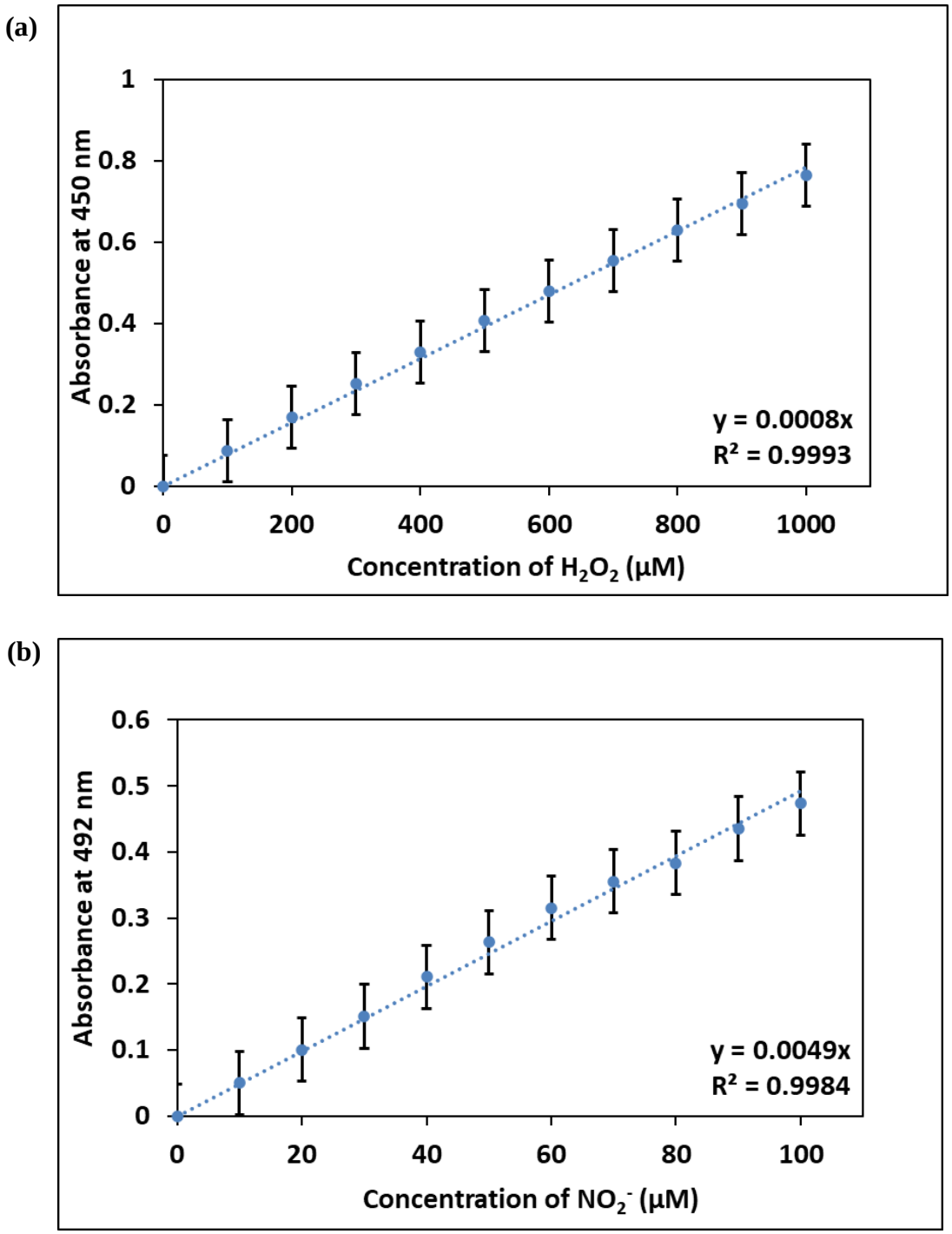

Figure S9: Calibration curves used to calculate the concentration of (a) H_2O_2 and (b) NO_2^-.

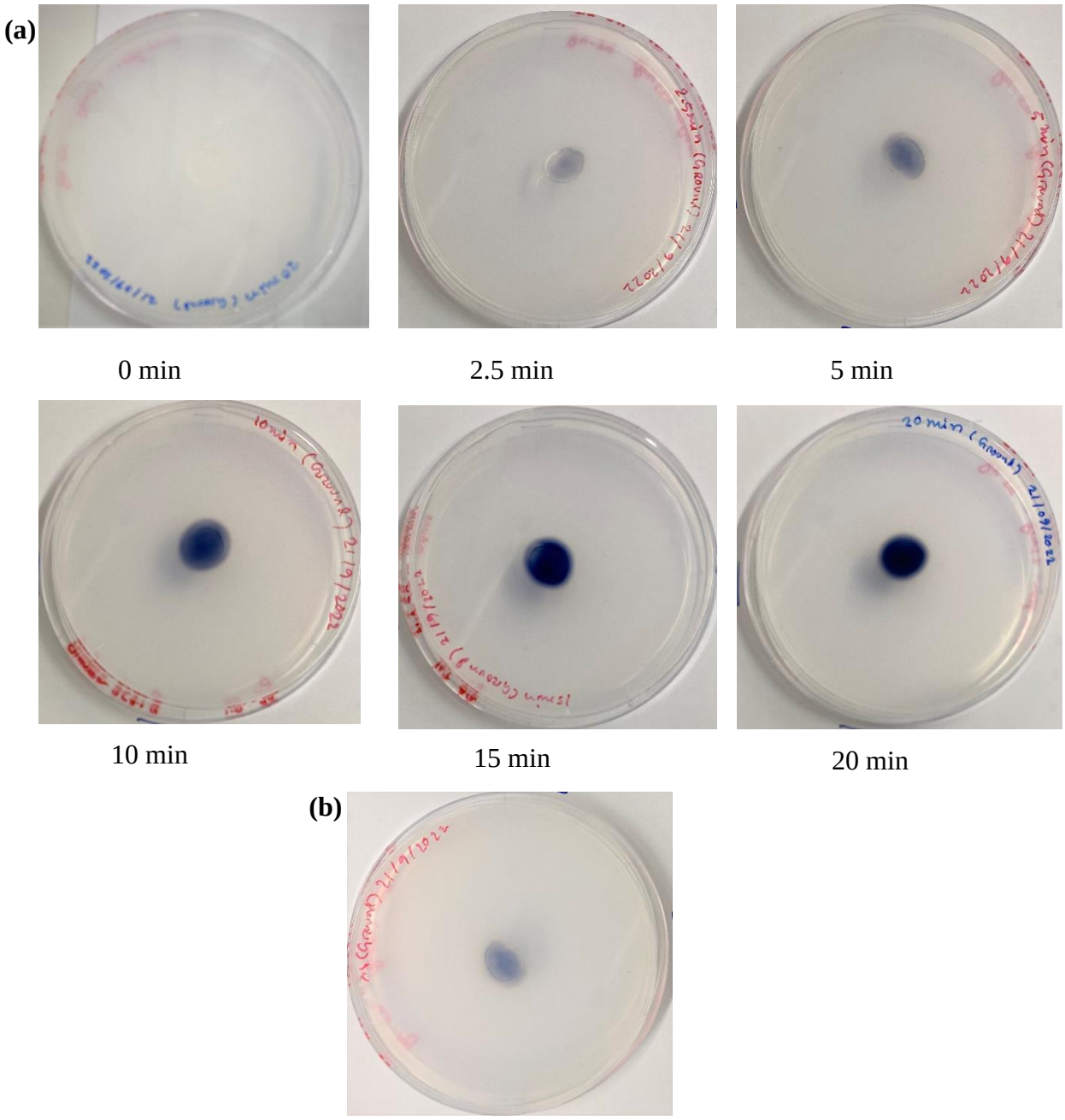

Figure S10: Photographs of the petri dish used in Figure 7(a). (a) PVA-FLT-W sample at different treatment times, and (b) PVA-FLT-W at 20 min treatment time.

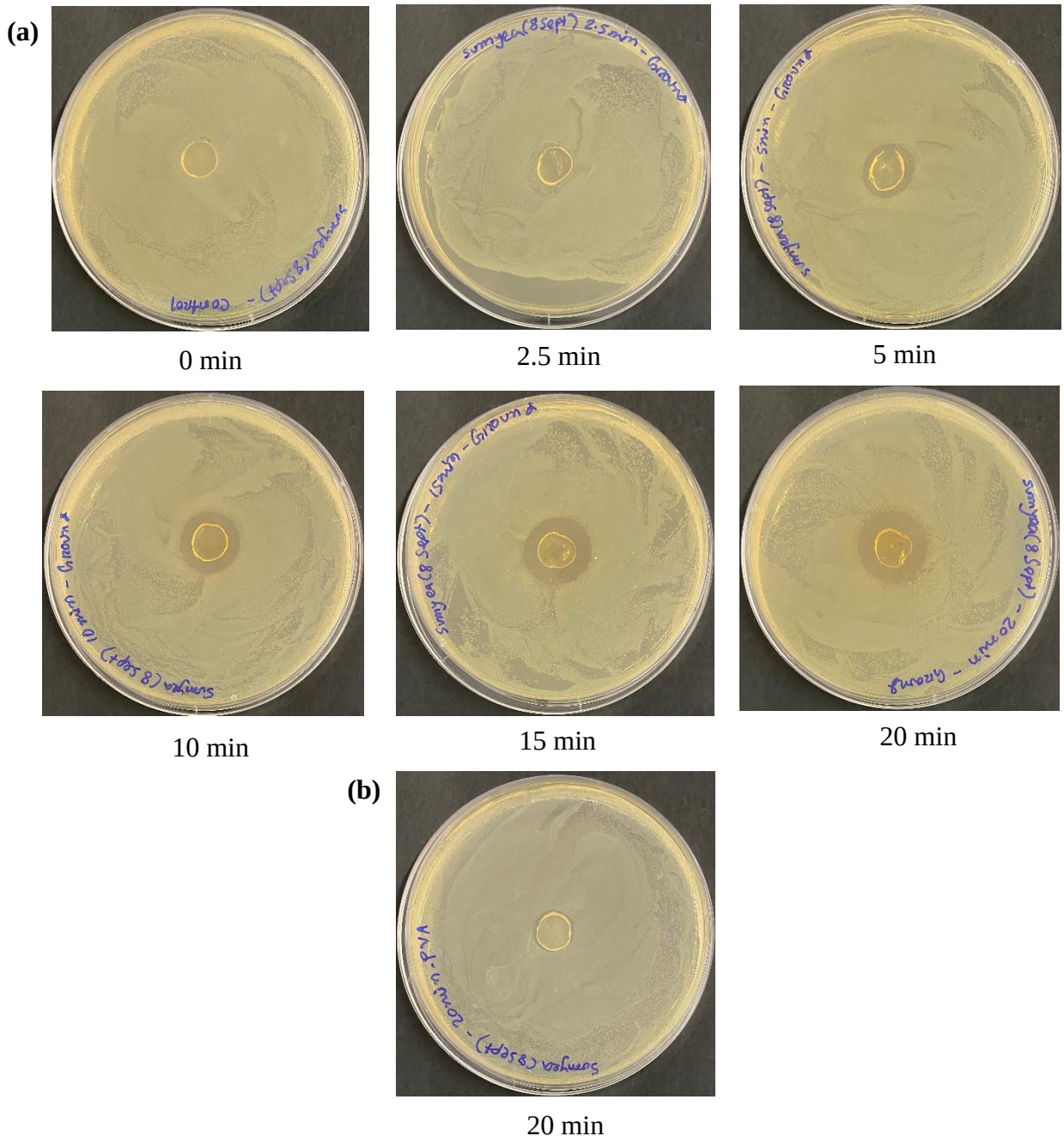

Figure S11: Photographs of the petri dish used in Figure 7 (a). (a) PVA-FLT-W sample at different treatment times, and (b) PVA-FLT-W at 20 min treatment time.

Day 0

Day 2

Day 7

Day 10

Figure S12: Photographs of the petri dish used in Figure 7 (b).

Untreated PVA

PVA-FLT-W

PVA-GND-W

Figure S13: Photographs of the petri dish used in Figure 7(c).

Untreated PVA PVA-FLT-W PVA-GND-W

Figure S14: Photographs of the petri dish used in Figure 7(d).

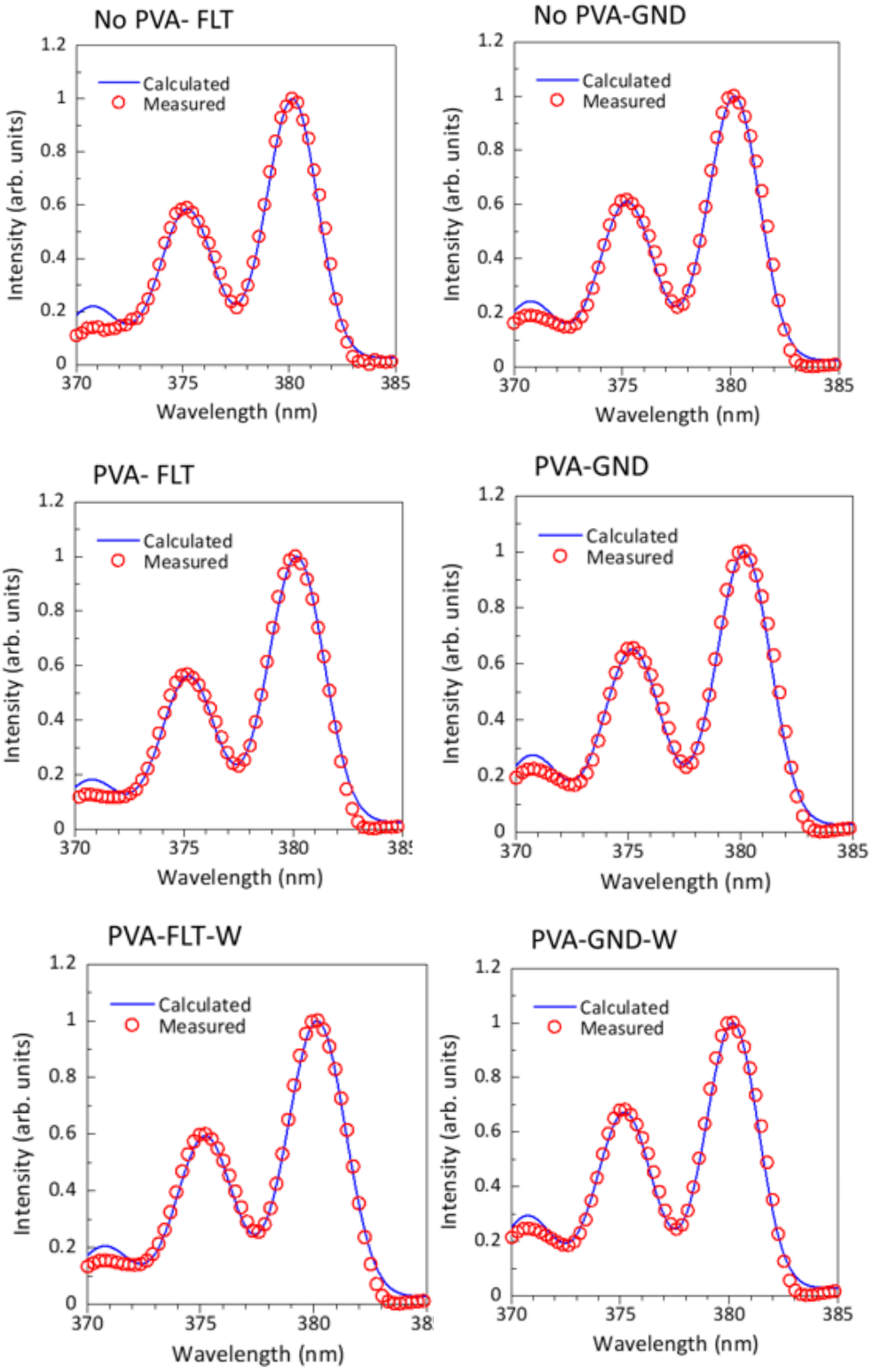

Figure S15: Measured OES (open circles) with the calculated spectrum (fitted line) from the spectrum simulator of the N_2 second positive system. The fitting procedure was used to calculate the vibrational and rotational temperatures presented in Table 5.